

AERO 481 Critical Design Report

December 9, 2018



Team 8 Air Infinity

Changqing Lu
Ruowen Tu
Jiadi Zhang
Yichen Zhou



Contents

1	Summary	4
1.1	Executive Summary	4
1.2	Dimensioned Three-view Drawings	5
1.3	Comparison Table	6
2	Introduction	6
3	Interior Layout	6
3.1	Cabin design	7
3.2	Cockpit Design	8
3.3	Baggage Location	9
3.4	Battery arrangement	11
3.5	Ladder installation	11
4	Aerodynamics	11
4.1	Drag Polar	11
4.2	Airfoil Selection	12
4.3	Wing Geometry	13
4.4	Stall Analysis	14
4.5	Cruise	18
4.6	Comments on AVL	18
5	Weights and Center of Gravity	19
5.1	Refined Weight and CG Estimates	19
5.2	CG Excursion	20
6	Control and Stability	21
6.1	Static Margin	21
6.2	Empennage	22
6.3	Rudder Sizing for OEI	22
7	Propulsion System	23
7.1	Motor Selection	23
7.2	Motor Integration	24
7.3	Propeller Selection	24
8	Landing Gear	25
8.1	Landing Gear System and Configuration	25
8.2	Preliminary landing gear and strut disposition	25
8.3	Tire Sizing	25
8.4	Retraction Kinematics	25
9	Method Validation	27
10	Objective Function	29
11	Design Refinement	29
11.1	Cruise Speed Trade Study	30

11.2	Altitude Trade Study	30
11.3	Climb and Descent Angles Trade Study	30
11.4	Aspect Ratio Trade Study	31
11.5	Taper Ratio Trade Study	32
11.6	Incidence and Twist Angles Trade Study	32
12	Final Sizing	34
12.1	P-S Diagram	34
12.2	Refinement Comparison Table	34
13	Structure	35
13.1	Load paths	35
13.2	V-n diagram	36
13.3	Distribution of Air Loads on the Wing	40
14	Cost	40
15	Computation Procedure	42
15.1	Optimization Process	42
15.2	Improved Estimation	43
15.3	Python Module Breakdown	43
15.4	Python Module Interaction	44
16	Conclusions	44
17	References	45
18	Appendix	46
18.1	List of Symbols	46
18.2	Supplementary Drawings	47
18.3	Supplementary Equations	47
18.3.1	Direct Operating Cost Equation	47
18.3.2	Weights and CG Location Estimates Equation	48
18.3.3	Stability Equation	48
18.3.4	V-n diagram equation	49
18.4	Supplementary Tables or Figures from Textbook	49

1 Summary

1.1 Executive Summary

This report introduces a refined electric short-range commuter type aircraft designed by Air Infinity. This is a small aircraft which is able to carry 9 passengers and a pilot travelling around Pacific Northwest region. The economic range of the plane is 250 *nmi* while the maximum range is 400 *nmi* with 100 *nmi* reserve. In this project, we compared two configurations of aircraft, electric configuration and conventional fuel configuration designed for PDR, and find out that the electric configuration for our mission provides a lower direct operating cost, which is our objective function. Thus we choose to further optimize electric configuration to minimize DOC. This report shows our effort and results we have got.

To optimize our design and achieve our goal to minimize the DOC, we integrate AVL into our design loop to calculate the induced and trim drag. We also use a gradient based method to find an optimal design point. The design parameters are cruise speed, cruise height, climb angle, descent angle, aspect ratio, taper ratio, incidence and twist. After finding the optimal design values, we do the trade study for each parameter to show a clearer view of the influence of these parameters on DOC.

The final optimized shape of our electric aircraft is shown in Figure 1, and the overall parameters of our electric aircraft are listed in Table 1. Our electric aircraft has a similar maximum takeoff weight as King Air 350i, which is 16943 *lb* with a battery weight 6150 *lb*. The span of our aircraft is the longest among the comparison aircrafts. Moreover, after our optimization, our electric aircraft only need a total power 1500 *hp*, which is the least among comparison aircrafts. Also, the cruise speed we designed is 333.6 *knots* (0.57 Mach), which is achievable by a turboprop aircraft. Finally, our aircraft has a 9.79% static margin, which makes our aircraft stable and still maneuverable.

We use a single fuselage, two engines integrated in low wings, T-tail behind and a tricycle landing gear configuration for our design. The MTOW center of gravity is 16.9 *ft* from the nose cone and neutral point location is 17.42 *ft*.

In our interior layout, we can hold at most 9 passengers. There is a restroom behind the cabin. The baggage cabinet is behind the motor. To avoid baggage become too hot, we add a radiator and cooling air duct between motor and baggage section. The battery is under the deck between the nose gear and the wing. In the cockpit, the pilot has a downward view range 17.5 degrees and is able to see both wing tips, which meets visibility requirements.

Our optimized wing has an area of 330.2 *ft*². We choose NACA 23012 for the wing tip and NACA 23018 for the wing root by considering both aerodynamic and structural reasons. We have a refined twist -1.6 degrees and incidence 2.9 degrees. AVL analysis is used to validate high lifting devices design satisfies the stall requirement and control surfaces design satisfies one engine inoperative condition.

For our propulsion system, we choose two Magnix 751 *hp* electric motors for our electric configuration. The power density is 2.83 *hp/lb*. We integrate both motors into the wing.

Our aircraft structure and V-n diagrams are also taken into consideration and are shown in corresponding parts.

Finally, we compare the improvement of our CDR design from PDR design. The direct operating cost is reduced to 0.29 *\$/nmi/pax* from a value of 0.387 *\$/nmi/pax* for PDR design. Therefore, our optimization do give our electric aircraft a better performance and lower DOC.

1.2 Dimensioned Three-view Drawings

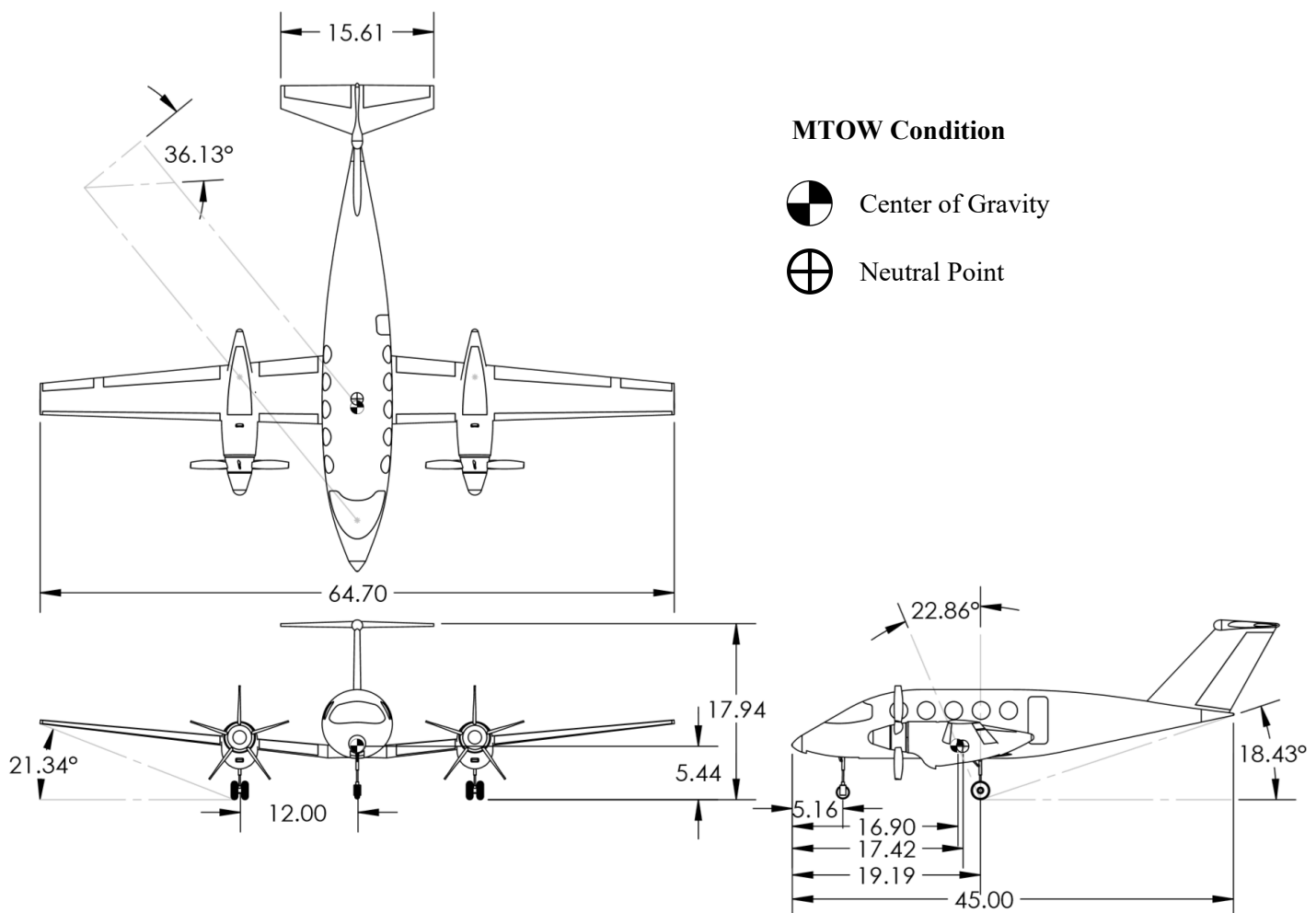


Figure 1. Three-view drawing for refined electric aircraft design.

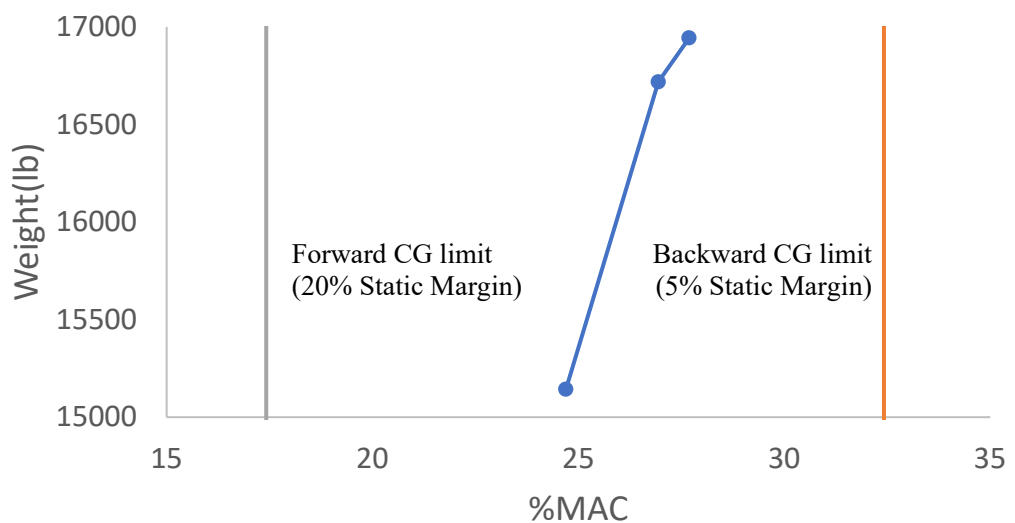


Figure 2. CG excursion for our electric aircraft.

1.3 Comparison Table

Here is our comparison table of our refined aircraft design and other three types of existing airplane: Zunum Aero, Beechcraft King Air 350i and Piaggio P.180 Avanti.

	Air Infinity CDR Electric Design	Zunum Aero	Beechcraft King Air 350i	Piaggio P.180 Avanti
MTOW [lbs]	16943	11500	15000	12100
Empty Weight [lbs]	8817	8402	9456	7850
Crew Weight [lbs]	175	175	350	350
Max Payload Weight [lbs]	1800	2500	2545	1750
P/W [hp/lbs]	0.089	0.117	0.140	0.140
W/S _{ref} [lbs/ft ²]	51.31	37.2	48.39	70.35
Engine type	Magnix Electric Motor	Series hybrid with range extender	Pratt Whitney PT6A-60A	Pratt Whitney PT6A-66B
Maximum Rated Power [hp]	751*2	1341	1050*2	850*2
Battery Weight [lbs]	6150	2300	N/A	N/A
SFC [lbs/hr/lbf]	N/A	N/A	0.548	0.620
Ext. length [ft]	45.0	42.0	41.6	41.3
Span [ft]	64.7	52	57.9	47.1
S _{ref} [ft ²]	330	309	310	172
Aspect Ratio	12.7	8.75	10.8	12.9
Average Wing t/c	15%	N/A	15%	N/A
Cruise Mach Number	0.57	0.45	0.47	0.60
Cruise L/D	14.4	N/A	N/A	N/A
Cruise/Landing/Takeoff C _L	0.398/2.18/2.49	N/A	N/A	N/A
Maximum Range [nmi]	400	700	1806	1490
Maximum Range Fuel [lbs]	N/A	800	3611	2802
Max # of Passengers	9	12	15	9
Static Margin	9.8%	N/A	N/A	N/A
Landing Distance [ft]	2336	2500	2692	2861
Take-off Distance [ft]	3440	2200	3300	2845

Table 1. Comparison Table for CDR & PDR Design.

2 Introduction

The objective of the mission is to design a commuter type airplane, whose entry-into-service date is 2030. It should satisfy Part 23 of the Federal Aviation Regulations. The economy range of the plane should be 250 *nmi* while the maximum range should be 400 *nmi* with 100 *nmi* reserve. What's more, the plane is supposed to carry 9 passengers and 1 pilot and each passenger is allowed to carry at most 25 *lbs* baggage. Here, we design two types of airplane. One uses electric propulsion and the other uses conventional fuel. After comparing their minimum direct operating cost at the same fixed mission, we choose electric configuration to be our final product.

3 Interior Layout

In this section, we will discuss the interior layout of Air Infinity based on the following parts: Cabin design, Cockpit Design, Baggage Location, Battery arrangement and Ladder installation. Figure 3 is the overview of our interior design.

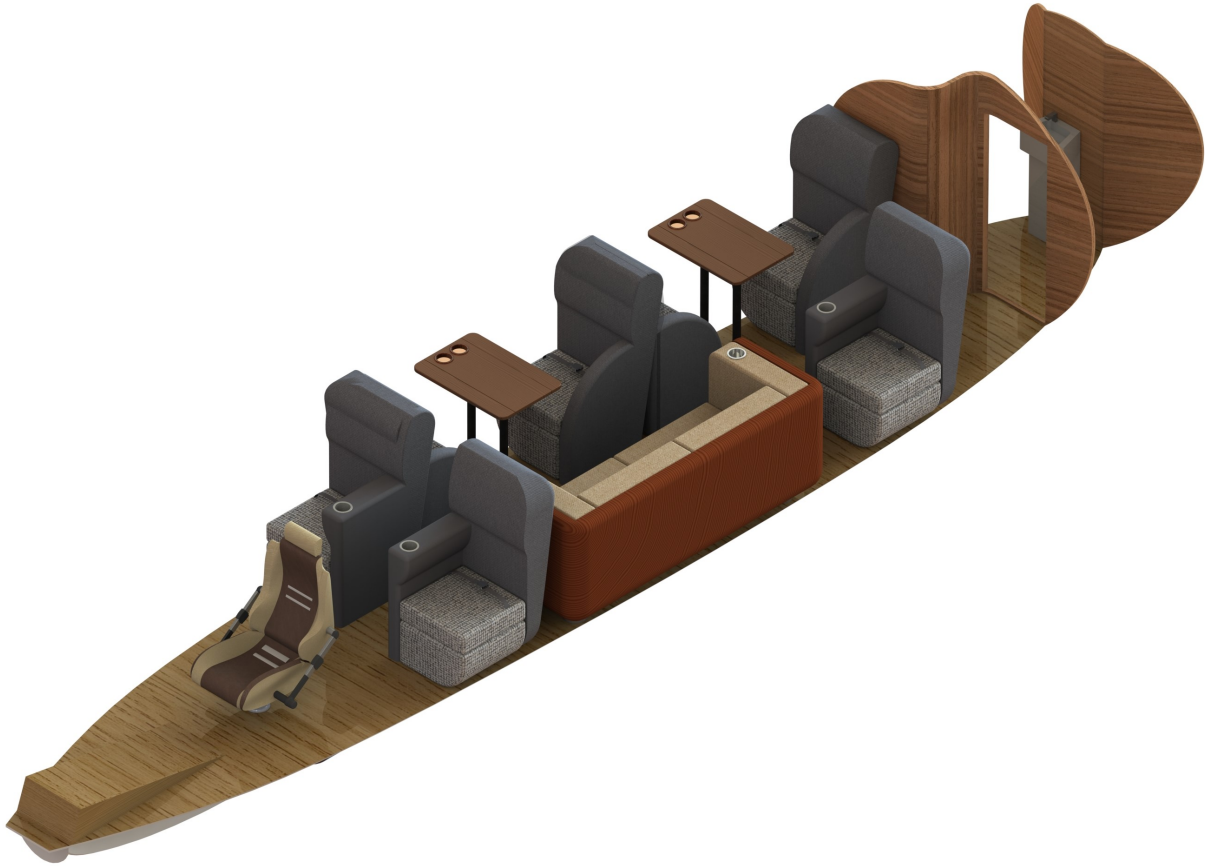


Figure 3. Overview of the interior layout.

3.1 Cabin design

A basic rendered view of cabin layout is shown in Figure 4. It contains totally 7 economy sofa and one luxurious sofa, which can hold at most 9 passengers. It also contains a restroom at the end of cabin. To ensure safety, each passenger has a safety belt and at least one cup holder in their seats.

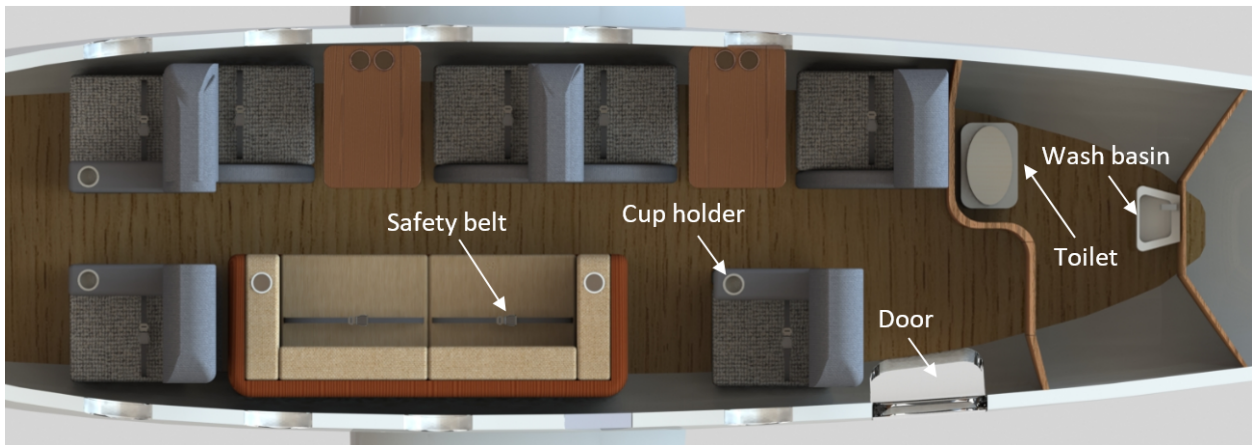


Figure 4. Top view of cabin layout.

In details, our cabin has a maximum height of 5.27 ft, a maximum width of 5.21 ft, and an active area of 118.18 ft², as displayed in side cross section view in Figure 5 and front cross section view in Figure 6. The

narrowest width of our aisle is 1.25 ft, which satisfies FAR 23.815. The wall thickness of our fuselage is 0.25 ft. It takes up more than 13.5% of our cross section, which is enough for the fuselage structures.

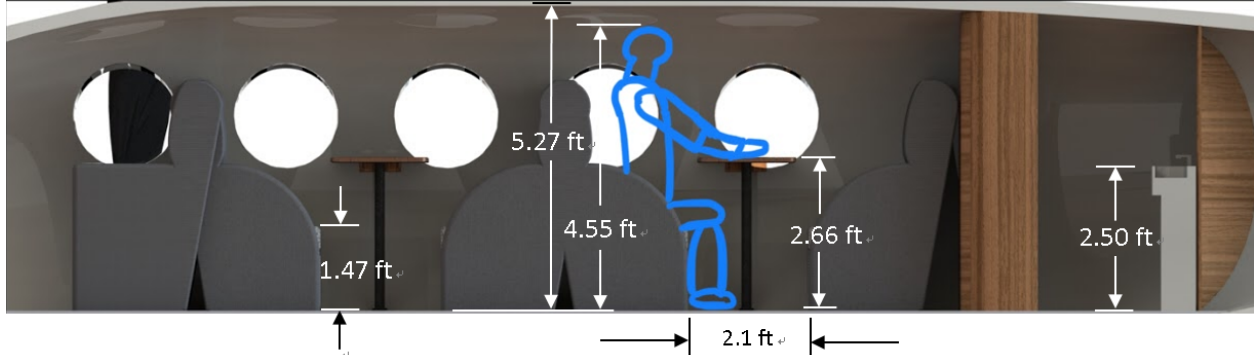


Figure 5. The floor of our cabin is higher than a sitting man and there is enough room for leg.

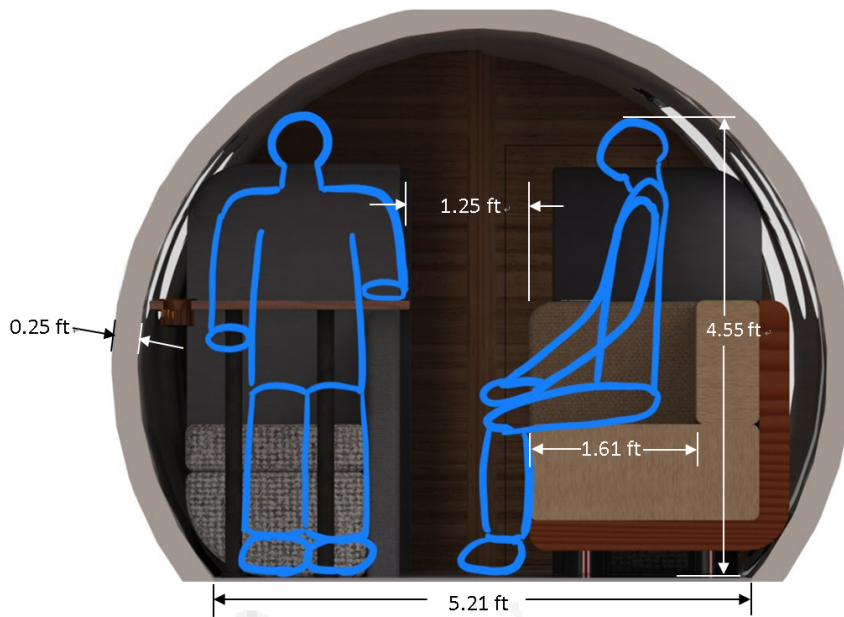


Figure 6. Aisle satisfies FAR 23 requirements and wall thickness is large enough for fuselage structures.

3.2 Cockpit Design

Air Infinity has a cockpit for one pilot, which contains an adjustable seat. So our pilot is able to adjust his view and control the plane easily, as shown in Figure 7. The vision angle is 55° up and 17.5° down. After subtracting the angle of attack, the exact angle below the horizontal line is still greater than 10° during takeoff. What's more, our pilot is able to see both aircraft wing tips through the windows in cockpit as shown in Figure 8.

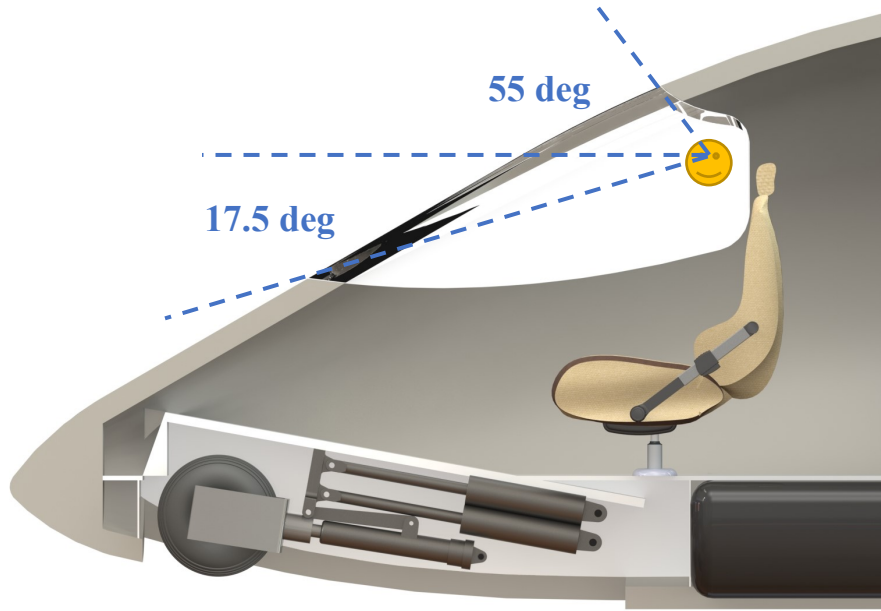


Figure 7. Pilot vision angle will be greater than 10° during climbing.

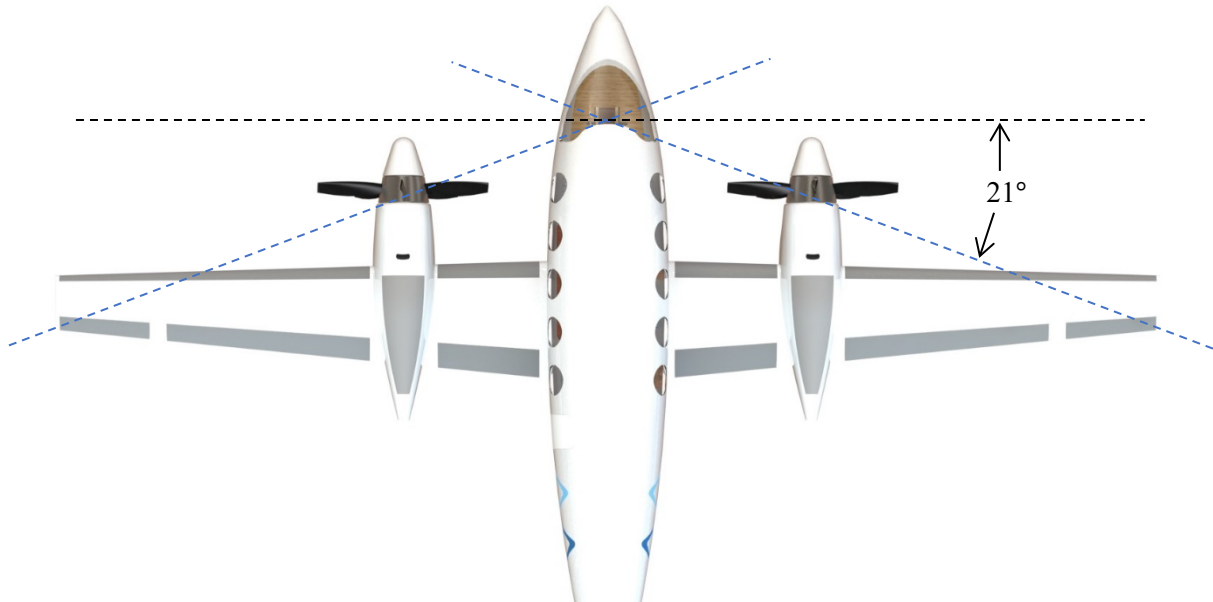


Figure 8. Our pilot is able to see both wing tips.

3.3 Baggage Location

Since we use electric motor instead of turbojets, there is enough room at the back of our nacelle. So we decided to put all the baggage at the back of our motors as shown in Figure 9. The total useable volume is more than 30 ft^3 , which also satisfies well with our baggage requirement.



Figure 9. Baggage location for the electric aircraft.

The detailed baggage section is in Figure 10 as below. We have a folded ladder at the back of the nacelle, which can be put down to the ground. Standing on the folder, passengers can put their baggage into the baggage section. And the lid can be automatically opened with the help of a hydraulic pole. Also, we add a radiator between the electric motor and baggage section. The heat generated by the motor will be took away by the cooling air, which can make sure the temperature in the baggage section will not be too high.

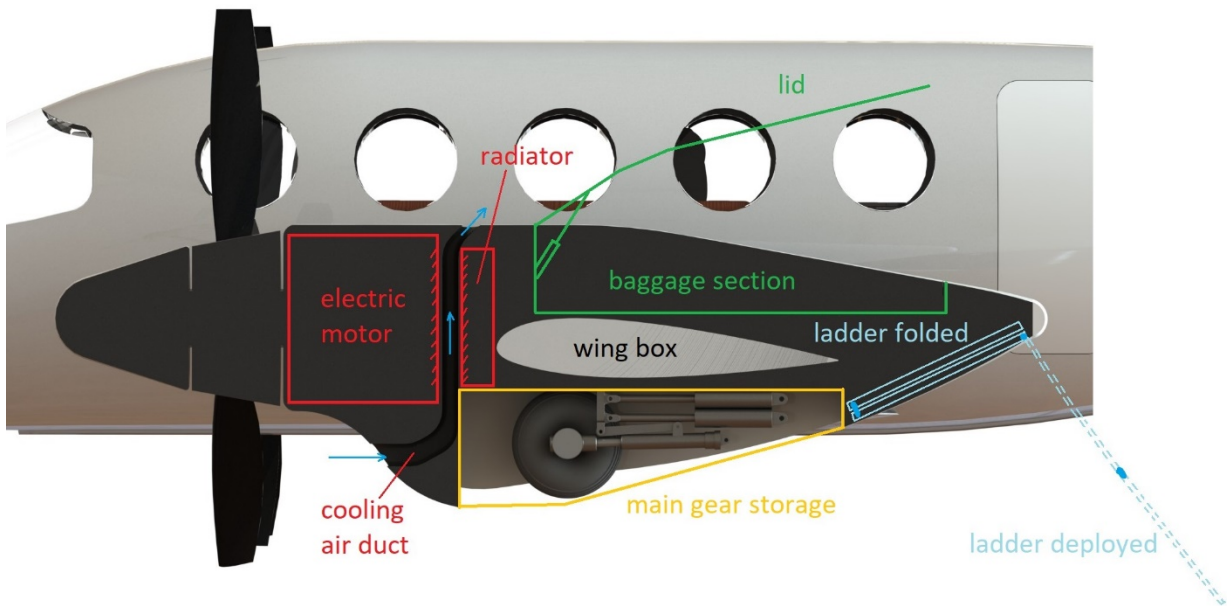


Figure 10. Baggage section interior design.

3.4 Battery arrangement

As shown in Table 1, the total mass of our battery is 6150 *lbs*. We assume the mass density of our battery to be 165 *lb/ft³*, so the volume of our battery is about 37 *ft³*. We design to put our batteries underneath the deck, where one is between the nose gear and the wing, and the other one is behind the wing as shown in Figure 11. This will make it easy for us to change and maintain them.

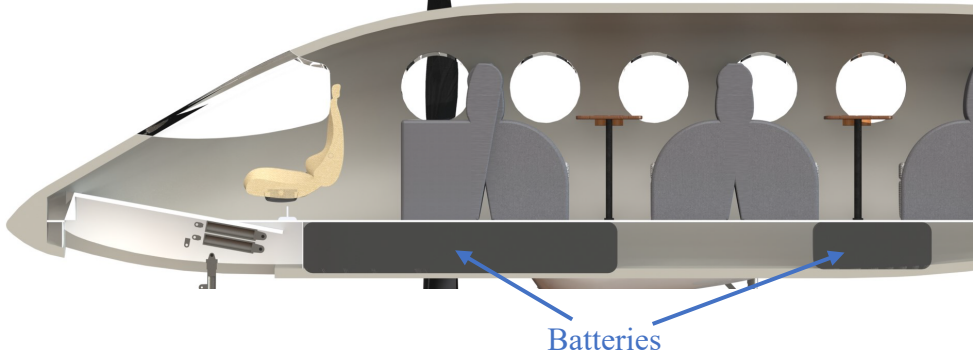


Figure 11. Battery position.

3.5 Ladder installation

We mount our ladder on the door of our fuselage as shown in Figure 12 below. So that our passengers can get into our plane without any extra help. The three landing gear hydraulic poles can change the height of our fuselage and make it easy for our passengers to reach the ladder.



Figure 12. Ladder is mounted on the door.

4 Aerodynamics

4.1 Drag Polar

After preliminary design, the refinement of aerodynamics are done for optimization. For different flight stages: cruise, climb, takeoff and landing as well as different flap/slat configurations, we can estimate drag polar for the whole aircraft.

Using AVL analysis, at different angle of attack, the relationship between the drag coefficient C_D and lift coefficient C_L at cruise (clean sheet) is calculated and a quadratic curve fitting is applied to have an analytic function with three coefficients. Then for individual configurations, C_{D_0} is calculated. For different flap and

slat configurations, ΔC_D and ΔC_L is introduced due to increase in drag and lift due to the setup of flaps and slats.

For clean sheet cruise scenario, we can estimate the function as

$$C_D = \frac{C_L^2}{\pi A Re} + b C_L + c$$

where b and c are constants calculated from curve fitting. Then we can calculate the lift efficiency e for clean sheet cruise scenario. By changing the flaps and slats using AVL, we can estimate Δe introduced by the setup of the flaps and slats and then using the corrected lift efficiency in the analytic function for other configurations. The Δe for takeoff is 0.095 while Δe for landing is 0.089, which are both close to typical values.

With calculated C_{D_0} , ΔC_D , ΔC_L and the corrected e , the original analytic function of $C_D = C_D(C_L)$ is then translated to the $C_L - C_D$ relationships for other configurations. Figure 13 below is the estimated drag polar for the final aircraft design. The maximum L/D is 18.7, which is indicated as the black dashed line while the operating L/D is 14.4, with C_L being 0.4.

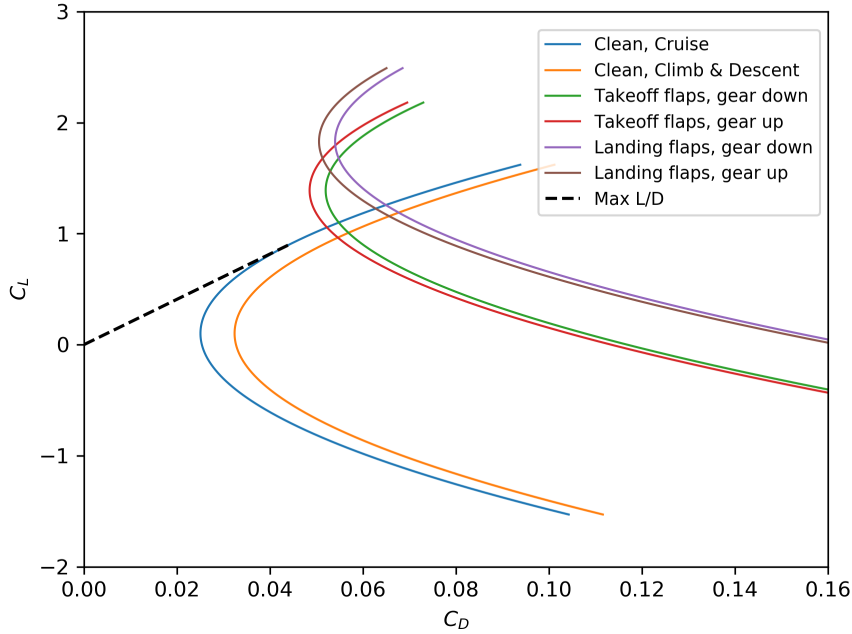


Figure 13. Drag polar.

As we can see from Figure 13, the maximum value for C_L is 1.62 for cruise, 2.18 for takeoff, 2.49 for landing, which are calculated based on a $Re \approx 9 \times 10^6$. Validation for stall are in the Stall Analysis.

4.2 Airfoil Selection

For the wing of both designs, we have selected two airfoils for root and tip respectively. For the root, NACA 23018 is selected and for the wing tip, NACA 23012 is selected. The geometries for both airfoils are shown in Figure 14 and Figure 15.

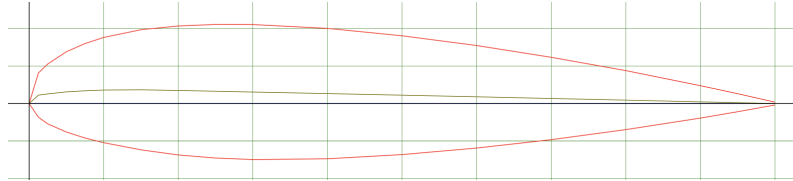


Figure 14. NACA 23018 Airfoil (root).



Figure 15. NACA 23012 Airfoil (tip).

This choice is based on the design of the Beechcraft King Air 350. The thickness-to-chord ratio, t/c , of NACA 23018 is 0.18 at 30% of the chord length. The t/c of NACA 23012 is 0.12 at 30% of the chord length. Therefore, we can expect a thickness decrease from root to tip.

When t/c of the airfoil decreases, the C_D of the wing will decrease because thinner airfoils produce less interference to the incoming flow and thus introduces less induced drag. Therefore, compared to a wing with sectional airfoil NACA 23018, C_D of the wing with two airfoils is reduced due to the decrease in sectional airfoil thickness. The lift efficiency with a thinner airfoil at the tip is increased as well.

The reason to maintain a thicker airfoil at the root is for structural consideration. A thicker airfoil leads to a structure with less weight and is able to take high bending moments at the root.

4.3 Wing Geometry

After finalizing the aerodynamics, we have the final design for wing. Figure 16 below shows the geometry of the wing.

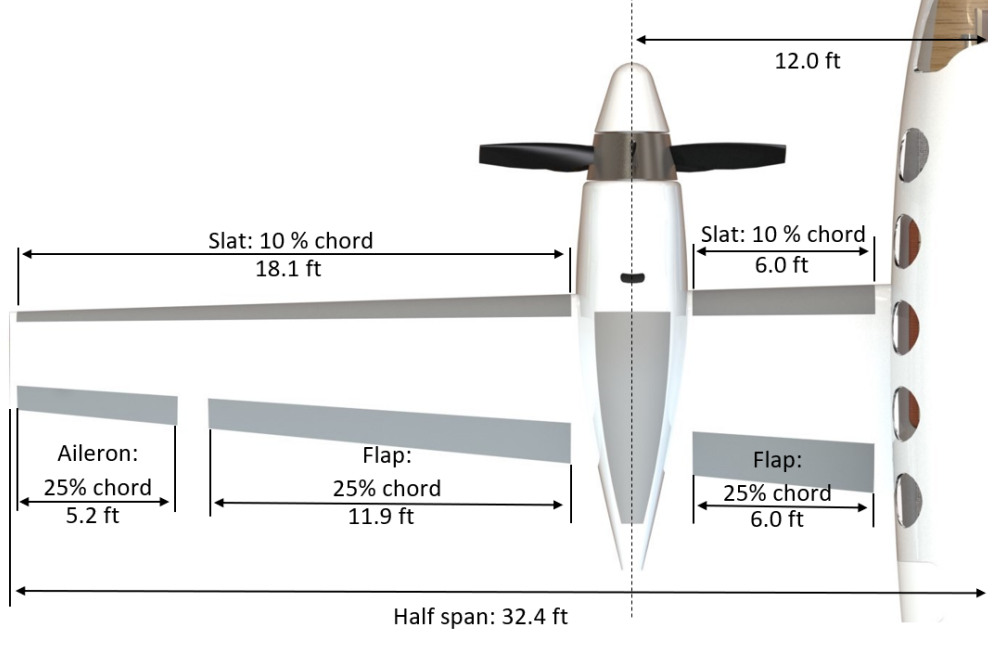


Figure 16. Electric Aircraft Wing Geometry.

The specifications for the wing is listed in the table below (Table 2).

Specifications	Value
Area [ft^2]	330
Aspect Ratio	12.67
Root Chord $c_r[ft]$	7.04
Taper Ratio λ	0.454
Span $b[ft]$	64.8
Incidence [deg]	2.9
Twist [deg]	-1.6
Sweep [deg]	0
Dihedral [deg]	6

Table 2. Electric Aircraft Wing Specifications.

Compared to the design from the preliminary stage, the area of wing stays the same as $330 ft^2$. A constraint of the span of the wing is applied so that the span does not exceed the 90% of the width of the runway ($\sim 75 ft$). Therefore, the aspect ratio increases from 10 to 12.67. Taper ratio decreases from 0.5 to 0.454 based on the optimization result as well as the trade study.

The flaps decreases from 30% chord to 25% chord since during aerodynamic analysis, we find that with 25% chord, the maximum lift coefficient $C_{L,max}$ can be reached for different configurations with reasonable deflection angle of 25° . Note that both the slats and flaps are separated for the position of the nacelle, which will introduce a lift decrease in the nacelle region.

4.4 Stall Analysis

To validate the geometry of the wing, we can use AVL to analyze the lifting surfaces during landing and cruise.

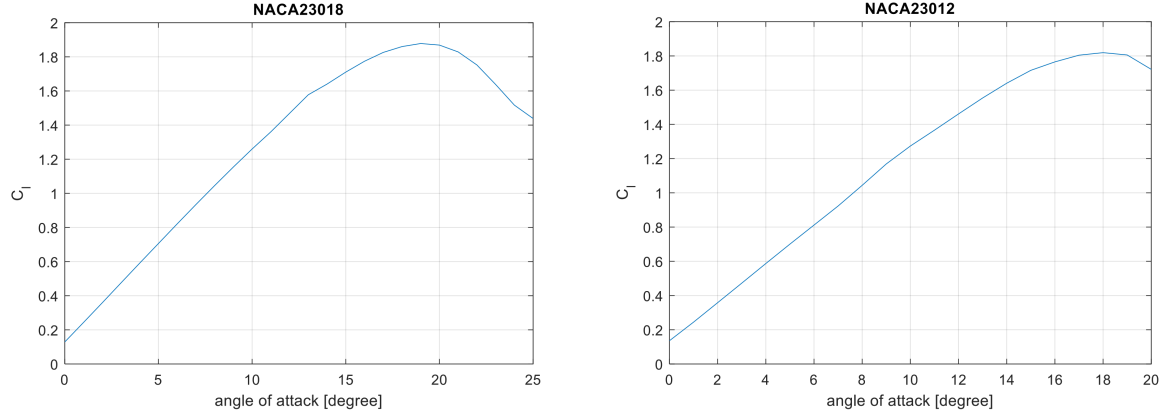


Figure 17. c_l vs. α for Selected Airfoils.

As we can see from Figure 17, we can see that the maximum sectional lift coefficient for NACA 23018 is around 1.9 and the maximum c_l for NACA 23012 is around 1.8. These c_l are airfoils without flaps or slats deployed. To more accurately estimate the sectional c_l for the wing, we need to take into account for the lift contribution of flaps and slats in high-lift scenarios such as takeoff and landing. Given the slats and flaps design, we can estimate the contribution of lift coefficient using equation,

$$\Delta C_{L,max} = 0.9 \Delta C_{l,max} \left(\frac{S_{flapped}}{S_{ref}} \right) \cos \Lambda_{HL}$$

where $\Delta C_{l,max}$ is selected based on Table 12 in Appendix. The results lead to different value of $C_{L,max}$ at different configurations.

To confirm wing does not encounter stall for all configurations, we need to compare the sectional lift coefficient C_l with $C_{l,max}$.

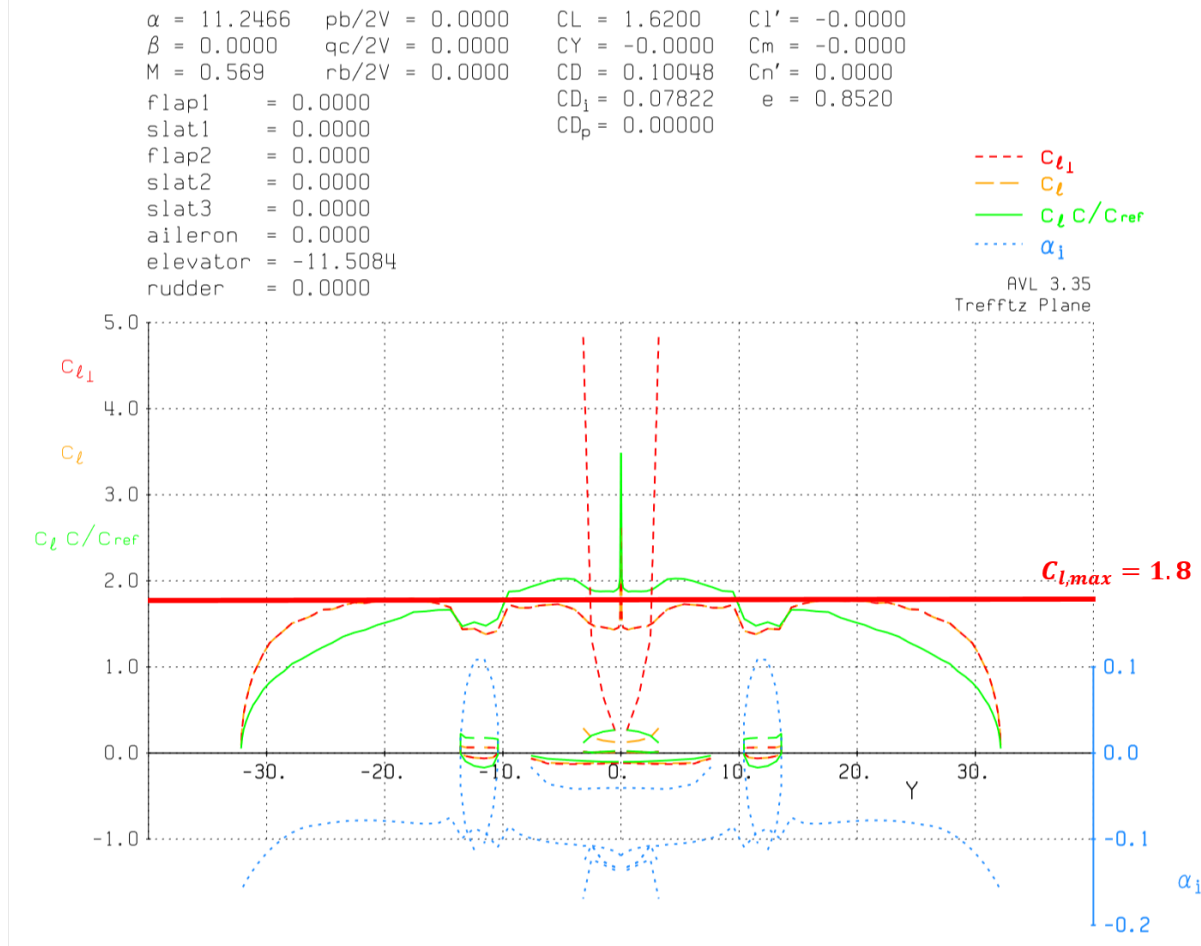


Figure 18. Cruise - Stall Analysis

For cruise, $C_{l,max} = 1.62$ while we compare sectional lift coefficient with 1.8, which is for clean sheet configuration. As we can see from Figure 18, around 20 ft of the wing, the sectional lift coefficient hit its maximum value, which means that even when the total lift coefficient is its maximum, the wing does not stall. Similar analysis are carried out for landing and takeoff cases.

```

 $\alpha = 12.9655$   $pb/2V = 0.0000$   $CL = 2.1800$   $Cl' = -0.0000$ 
 $\beta = 0.0000$   $qc/2V = 0.0000$   $CY = -0.0000$   $Cm = -0.0000$ 
 $M = 0.132$   $rb/2V = 0.0000$   $CD = 0.21483$   $Cn' = 0.0000$ 
flap1 = 25.0000  $CD_1 = 0.19470$   $e = 0.6331$ 
slat1 = 0.0000  $CD_p = 0.00000$ 
flap2 = 25.0000
slat2 = 0.0000
slat3 = 0.0000
aileron = 0.0000
elevator = -16.4685
rudder = 0.0000

```

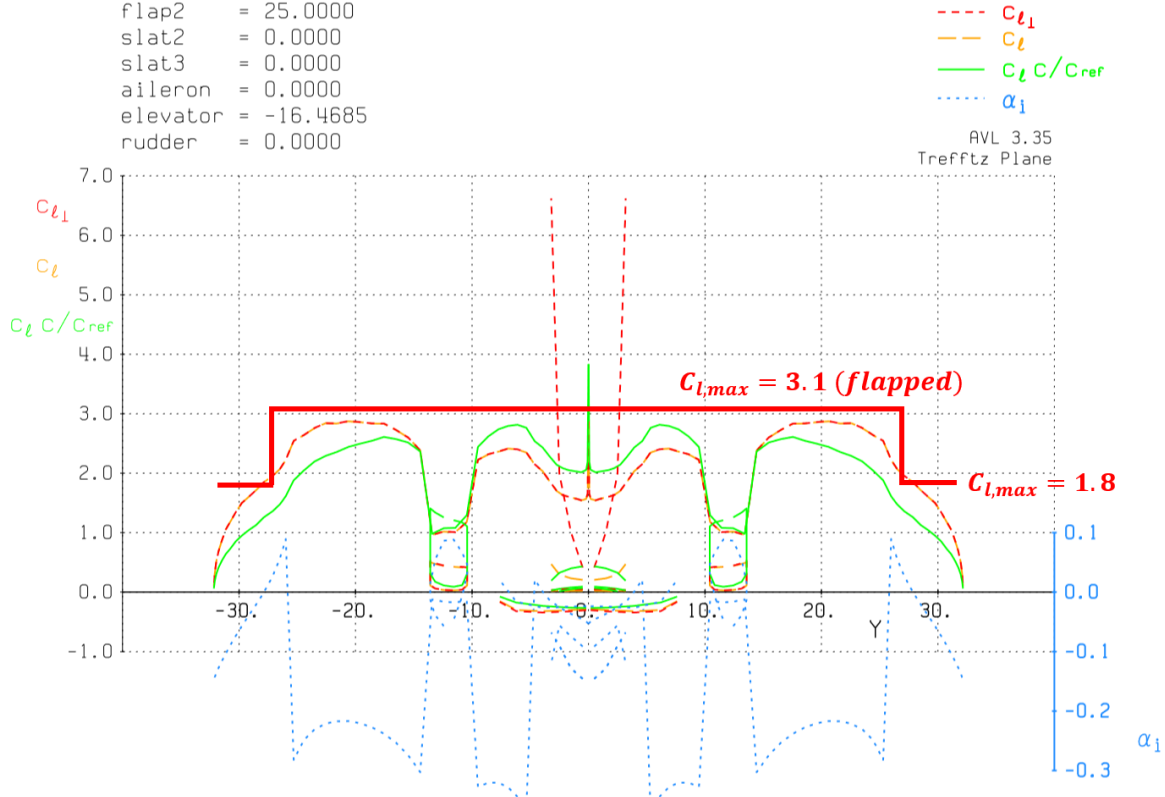


Figure 19. Takeoff - Stall Analysis.

For takeoff, the flaps are set at 25 degree deflection, the Mach number is recalculated according to the air density near ground and the speed. The sectional lift coefficient maximum value for regions with high lift devices are 3.1. Since according to the design, most of the area of the wing are flap-covered, which leaves us to compare the aileron area with sectional lift coefficient of 1.8. As we can see from Figure 19, the wing does not encounter stall in this case as well.

```

 $\alpha = 16.2523$   $pb/2V = 0.0000$   $CL = 2.4900$   $Cl' = -0.0000$ 
 $\beta = 0.0000$   $qc/2V = 0.0000$   $CY = -0.0000$   $Cm = -0.0000$ 
 $M = 0.132$   $rb/2V = 0.0000$   $CD = 0.28259$   $Cn' = 0.0000$ 
 $flap1 = 25.0000$   $CD_i = 0.25686$   $e = 0.6390$ 
 $slat1 = 25.0000$   $CD_p = 0.00000$ 
 $flap2 = 25.0000$ 
 $slat2 = 25.0000$ 
 $slat3 = 25.0000$ 

```

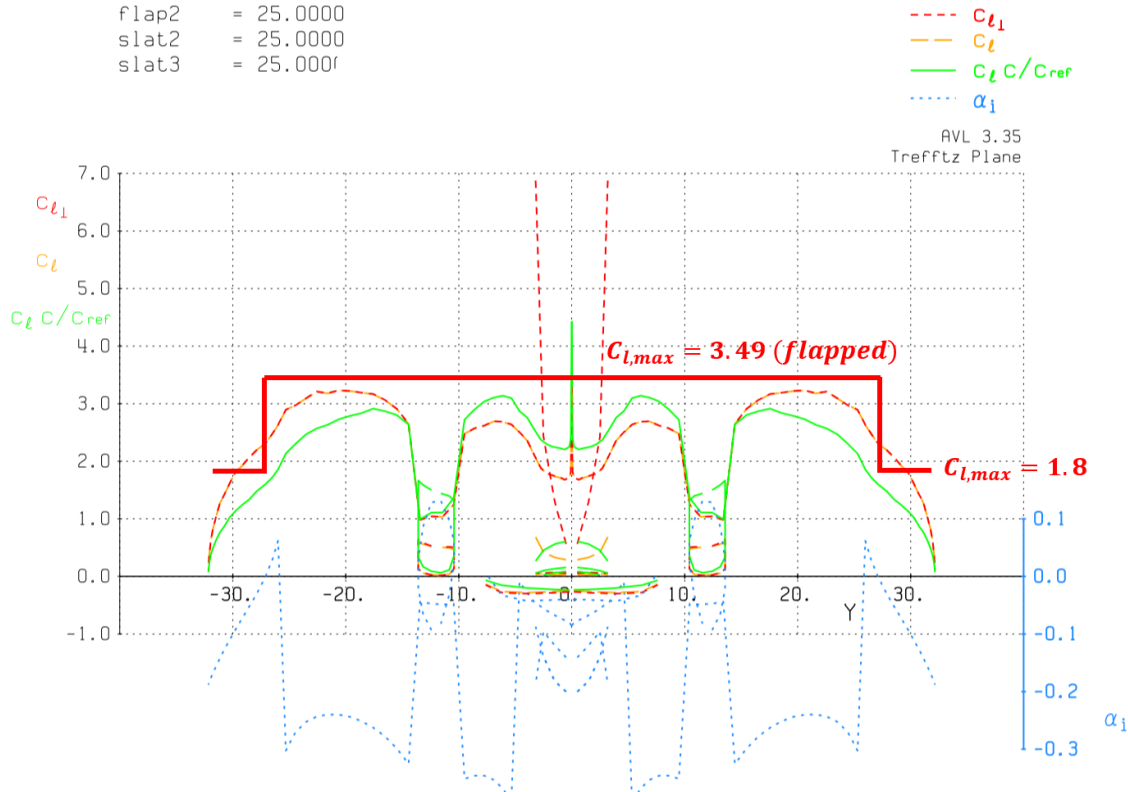


Figure 20. Landing - Stall Analysis.

At landing, slats are also deployed at 25 degree, which contributes to an increase in sectional lift coefficient of 0.3 for the whole wing since we have a leading edge approximately covering the wing. As we can see from Figure 20, the wing does not stall as well.

Using AVL, we can validate that the wing design does not introduce any stall during operation.

4.5 Cruise

```

 $\alpha = 0.6111$     $pb/2V = 0.0000$     $CL = 0.3980$     $C1' = -0.0000$   

 $\beta = 0.0000$     $qc/2V = 0.0000$     $CY = -0.0000$     $Cm = -0.0000$   

 $M = 0.000$       $rb/2V = 0.0000$     $CD = 0.00306$    $Cn' = -0.0000$   

 $flap1 = 0.0000$     $CD_1 = 0.00243$     $e = 1.6300$   

 $slat1 = 0.0000$     $CD_p = 0.00000$   

 $flap2 = 0.0000$   

 $slat2 = 0.0000$   

 $slat3 = 0.0000$   

 $aileron = 0.0000$   

 $elevator = -1.6370$   

 $rudder = 0.0000$ 

```

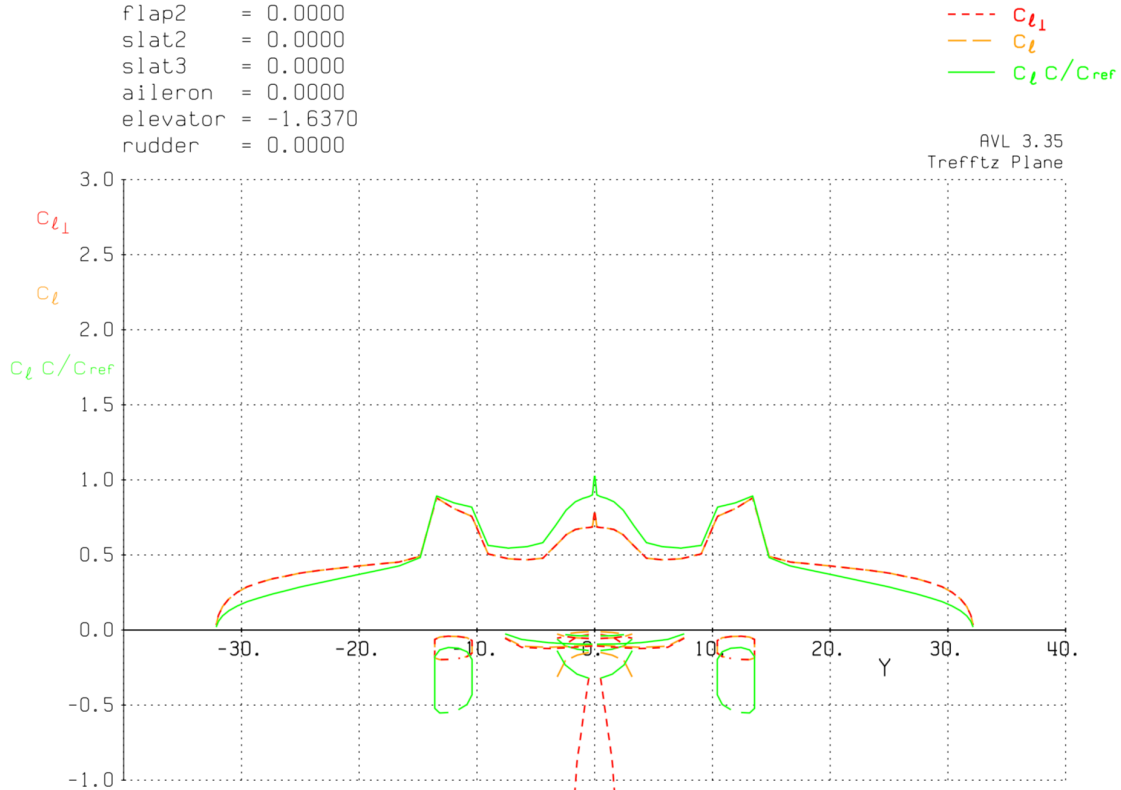


Figure 21. Cruise Aerodynamic Analysis.

Using the finalized weight, the cruise speed and the cruise height, we can calculate the dynamic pressure of the cruise condition. Then with the finalized wing area, we can calculate the operating lift coefficient, which is around 0.4. Compared to similar aircraft, the lift coefficient is relatively low. However, the high cruise speed can compensate the lift coefficient. Note that with the drag polar shown in Figure 13, the operating lift-to-drag ratio is 14.4 while the maximum lift-to-drag ratio is around 18.7. Although the aircraft is not operating in the optimal lift-to-drag ratio, which leads to a higher consumption of power to counteract drag, the aircraft flying at high speed means that the time spent is less, which would decrease the direct operating cost. In short, there is a trade-off between the cruise speed and drag.

4.6 Comments on AVL

Using AVL is a convenient way to analyze the aerodynamic aspect of the aircraft. Wings, fuselage, empennage as well as nacelle can be integrated as panel models into the analysis of AVL. But the results of the analysis are limited in some sense.

First of all, AVL analysis is sensitive to the number of spanwise panels. For complex configuration with multiple sections for high lift device setup, when the spanwise panel number is appropriate, the results of AVL can show relatively correct trends while when the spanwise panel number is too large, the results are not reasonable. In Figure 22, the left plot shows the AVL results for a flapped and slatted wing with 100 spanwise panels while the right plot shows one with 30 panels. The lifting line on the left plot shows

zigzag patterns that is due to the precision of the panel number. The right plot is more reasonable because the lifting line is more continuous and smoother.

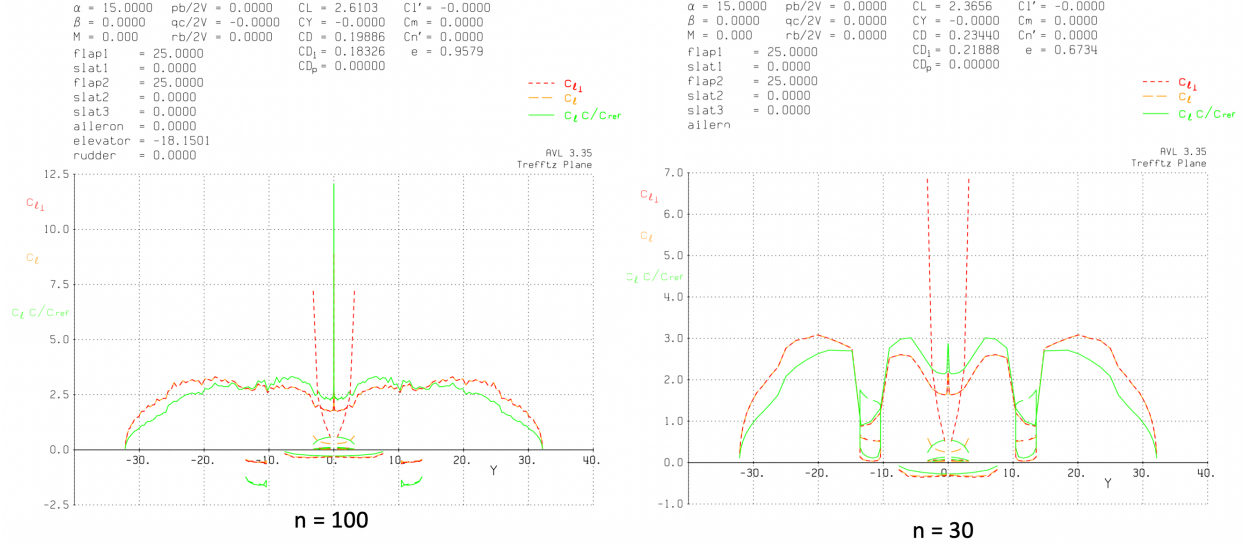


Figure 22. Panel number comparison.

Secondly, the lift and drag coefficients for the whole aircraft with high lift device cannot be used as precise calculation results since the panel method is not accurate enough for flap and slat configurations since the number of spanwise panels is limited and the total lift and drag coefficients can only be integrated from the discontinuous panels. Therefore, when updating the refined drag polar, we translated the results of clean sheet model to calculate for high lift device configurations.

5 Weights and Center of Gravity

5.1 Refined Weight and CG Estimates

We use a more accurate method to estimate the CG location, which is detailed component weights method. First, we breakdown the total weight into twelve components: fuselage, wing, horizontal tail, vertical tail, motor, noes landing gear, main landing gear, fixed equipment, battery, crew, passengers and baggage. For fuselage, tails, landing gears and fixed equipment weights are referred to Table 13 for transport aircraft in Appendix 18.4, which is provided by Raymer. We adjust the percentage of fixed equipment from 17% of MTOW to 22% MTOW since electric aircraft includes some battery related equipment. Besides, we also consider the fudge factors. We choose the smallest fudge factor in Table 14 in Appendix 18.4, which is also provided by Raymer. For wing, we apply two equations from Raymer and Kroo (18.3.2), then take the average to get the wing weight. For motor weight, we use a power density of 2.83 hp/lb to calculate the weight. The electric motors we selected have a total rated power 1502 hp , which gives a motor weight 530.74 lb . It should be mentioned that we use a correction factor 0.632 for tails and fuselage. It is obtained from a correction to King Air 350ER, which is an aircraft having similar mission. The final weight and CG location for each component is shown in Table 3.

Component	W(lbs)	x(ft)	Wx(lb·ft)	z(ft)	Wz(lb·ft)
fuselage	1991	20.25	40317.75	7	13937
wing	1490	17.15	25553.5	4.5	6705
horizontal tail	169.53	46	7798.26	16	2712.44
vertical tail	185.45	42	7789.02	11	2039.98
motor	530.74	12	6368.90	5	2653.71
landing gear nose	109.15	5.2	567.60	1.8	196.48
landing gear main	618.53	19.2	11875.88	1.8	1113.36
fixed eqp	3723.06	17.7	65898.16	7	26061.42
battery	6149.82	14	86097.45	3.8	23369.31
crew	175	7.15	1251.25	7	1225
passenger normal	1575	18	28350	7	11025
baggage wing	225	19.5	4387.5	5.2	1170
MTOW	16943	16.90	286255.28	5.44	92208.70

Table 3. Component weights breakdown and CG locations.

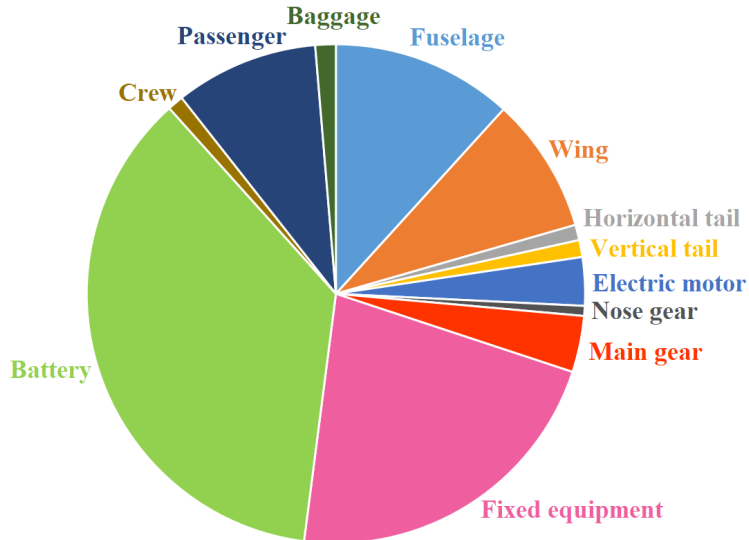


Figure 23. MTOW breakdown pie chart.

5.2 CG Excursion

From our component weight method, we get a more accurate estimate on CG location. Then we can plot the CG excursion. We set our backward CG limit to be 5% static margin to make sure that our aircraft is stable enough, and forward CG limit to be 20% static margin to make sure that our aircraft still has good maneuverability. The neutral point position and wing MAC are calculated and shown in next section 6.1. We mainly consider three weight configurations, which are MTOW, without baggage and without passenger and baggage. The plot is shown in Figure 24.

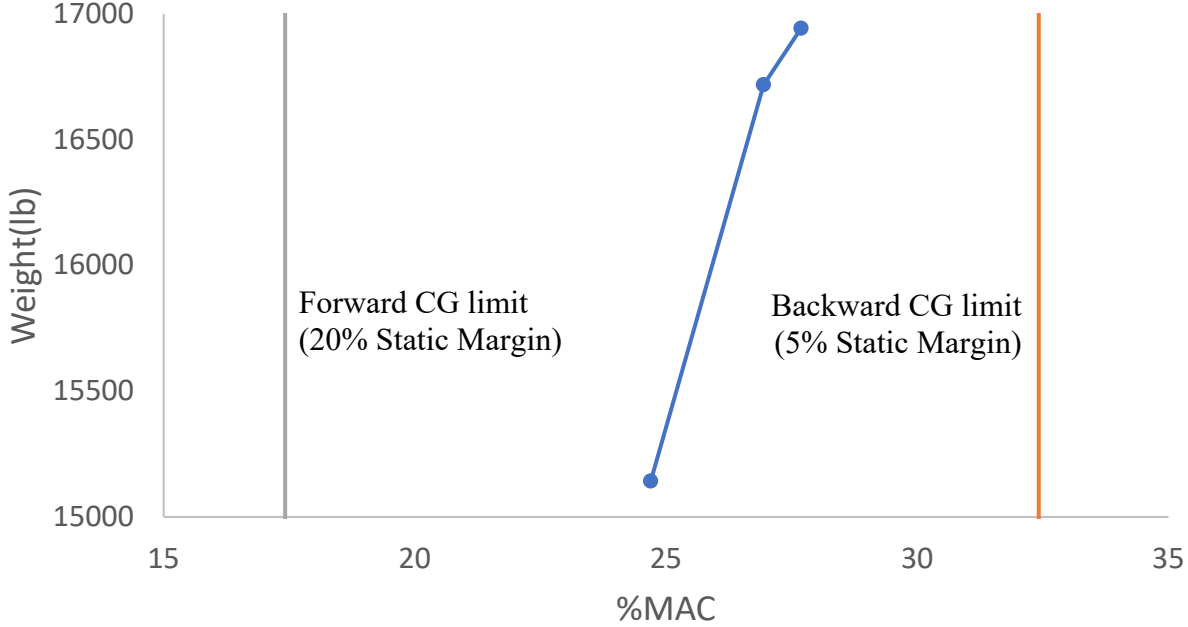


Figure 24. CG excursion in different weight configurations satisfy our CG limit requirements.

6 Control and Stability

In this section, we mainly discuss the static margin, empennage design and one engine inoperative condition. The static margin part includes MAC calculation.

6.1 Static Margin

Using the improved weight estimate method as described in section 5.1 Refined Weight and CG Estimates, we estimate the center of gravity of each component and their C.G. Location. Then using these values, we can estimate the center of gravity and neutral point location, thus getting the static margin.

We calculate the mean aerodynamic chord (MAC) for wing, vertical tail and horizontal tail. The equations are given by metabook:

$$\bar{c} = \frac{2}{3} c_{root} \frac{1 + \lambda + \lambda^2}{1 + \lambda}$$

$$X_{MAC} = X_{RLE} + \frac{b}{6} \frac{1 + 2\lambda}{1 + \lambda} \tan(\Lambda_{LE})$$

Applying corresponding values into these equations, we can get our wing MAC equals to 5.345 ft. Then we calculate the spanwise location using following equation:

$$\bar{Y} = \frac{b}{6} \frac{(1 + 2\lambda)}{(1 + \lambda)}$$

So our MAC's spanwise location is 14.15 ft from the center line. The neutral point and static margin are calculated using equations below and other detailed equations shown in 18.3.3.

$$\frac{x_{np}}{\bar{c}} = \frac{l_h S_h C_{Lah}}{\bar{c} S_w C_{Law}} - \frac{1}{C_{Law}} \frac{\partial C_{mfus}}{\partial \alpha}$$

$$\text{static margin} = \frac{x_{np} - x_{cg}}{\bar{c}}$$

Therefore, we get our $x_{np} = 17.42$ and static margin at MTOW is 9.794% MAC.

6.2 Empennage

The design of empennage refers to the empirical value of the volume coefficient and the correction factor for T-tail. The typical volume coefficient for horizontal tail is 0.9 and for vertical tail is 0.08. The correction factor for T-tail is 0.95. The equation to calculate the volume coefficient is defined as:

$$c_{VT} = \frac{L_{VT}S_{VT}}{b_W S_W}$$

$$c_{HT} = \frac{L_{HT}S_{HT}}{\overline{c_W} S_W}$$

Then we take stability into account. Since we have finished design our wing, we need to make sure that our empennage will give our aircraft a steady performance. The results are shown in Table 4. The actual dimension of our empennage is labeled in three-view drawings in Figure 25.

	Moment Arm[ft]	Reference Area [ft ²]	Aspect Ratio	Taper Ratio	Sweep [deg]	Volume Coefficient
Vertical Tail	23.4	69.37	2	0.5	30	0.0704
Horizontal Tail	24.75	60.97	4	0.5	15	0.824

Table 4. Empennage size and design.

The airfoils used for both vertical and horizontal tails are designed to be symmetric, since we do not want extra asymmetric moment exerts by the empennage on the aircraft. We choose NACA 0012 as our airfoil for the empennage.

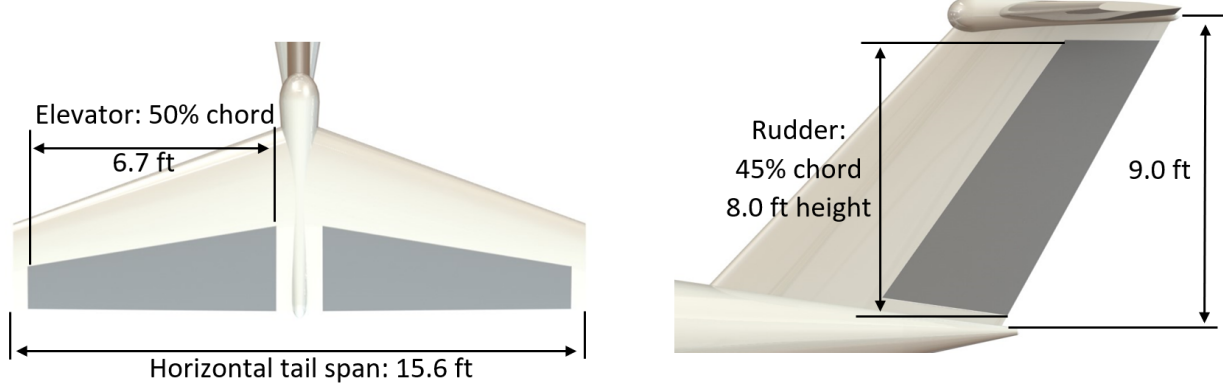


Figure 25. Empennage control surfaces design.

6.3 Rudder Sizing for OEI

We calculate the worst case for one engine inoperative condition, which is in takeoff with maximum power. First, we know that the yaw moment coefficient is defined as:

$$c_N = \frac{N}{qSb} = \frac{Tl_n}{qSb} = \frac{\eta Pl_n}{qSbV}$$

Where l_n is the moment arm for yaw moment, which is the distance between engine and center line. P is the power, and η is the propulsive efficiency, which is 70% during takeoff. S is the wing reference area and b is the wing span. V is the takeoff speed, approximate to be 1.2 times of stall speed during takeoff, which is 96 knot. The dynamic pressure, q, is $\frac{1}{2}\rho_{st}V^2$. Applying all the values into this equation, $c_N = 0.0344$.

Then use AVL to get the rudder deflection in trimmed flight condition. We validate that our rudder sizing is able to deal with worst OEI condition. The AVL result is shown in Figure 26.

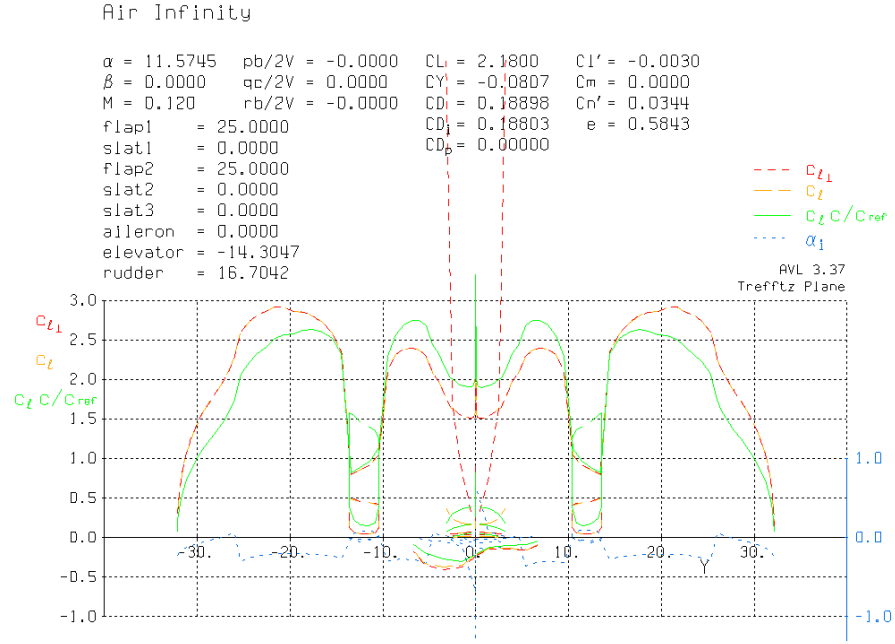


Figure 26. Rudder deflection angle is 16.7 degrees for OEI condition during takeoff.

The maximum rudder deflection is 16.7 degrees, which is achievable. Thus our rudder sizing and elevator sizing is feasible.

7 Propulsion System

7.1 Motor Selection

For our refined design of electric aircraft, two electric motors are selected. Our required takeoff power is around 1450 *hp* while current Magnix Magni500 motor can provide 751 *shp* with a power to weight ratio of 2.83 *hp/lbs* and 93.8% efficiency. Therefore, the power requirement of the design can be achieved with current technology. We simply choose to use two Magni500 electric motors for our electric aircraft. In the year of 2030, more advanced motors can be introduced with higher power to weight ratio, which may further decrease the direct operating cost.



Figure 27. Magni500 Motor^[21].

7.2 Motor Integration

We integrate our motors into the nacelles on the wing. The distance between the motor and the centerline of the airplane is 12 ft. The motor is placed at the front of the nacelle, which has a radiator and a cooling air duct behind it (Figure 10). We also integrate our main landing gear into the lower rear part of the nacelle. The upper part of the nacelle is baggage section. The radiator and cooling air can help to get rid of the heat generated by the motor and keep the baggage section under a preferable temperature.

7.3 Propeller Selection

We select two five-blade propellers for our electric aircraft. The diameter of the propeller is designed to be 10.5 ft. The design maximum RPM of the propeller is 2000 RPM. During the flight, the maximum thrust is required when the aircraft is taking off. We assume the power of each motor is set to be the maximum (751 hp), and the propulsive efficiency during takeoff is $\eta_p = 70\%$. The takeoff flight speed is assumed to be 1.2 times the stall speed. So we can calculate the required thrust for takeoff by the following equation:

$$T_{\text{required}} = \frac{P\eta_p}{1.2V_{\text{stall}}}$$

The required thrust is 1784 lbf for each propeller.

Then we can estimate the maximum thrust that our propeller can provide. Here we need to introduce power coefficient and thrust coefficient, which are defined as

$$C_{\text{pow}} = \frac{P}{\rho n^3 D^5}$$

$$C_T = \frac{T}{\rho n^2 D^4}$$

Where ρ is the air density, n is the rotation frequency in Hz and D is the propeller diameter. We calculate our power coefficient to be 0.039. According to Raymer's plot of the relationship between power coefficient and thrust coefficient for three-blade propeller (Figure 59 in Appendix), we can estimate the thrust coefficient for our five-blade by multiplying an adjustment factor of $(\frac{1}{95\%})^2$, which leads to the final thrust coefficient for our five-blade propeller to be 0.12. Then the maximum thrust each five-blade propeller can provide is 3600 lbf. This value is much larger than the thrust required by the takeoff stage, which means our propeller size is large enough to provide adequate thrust.

The propulsive efficiency we assume for takeoff is 70%, for climb is 85% and for cruise is 92%.

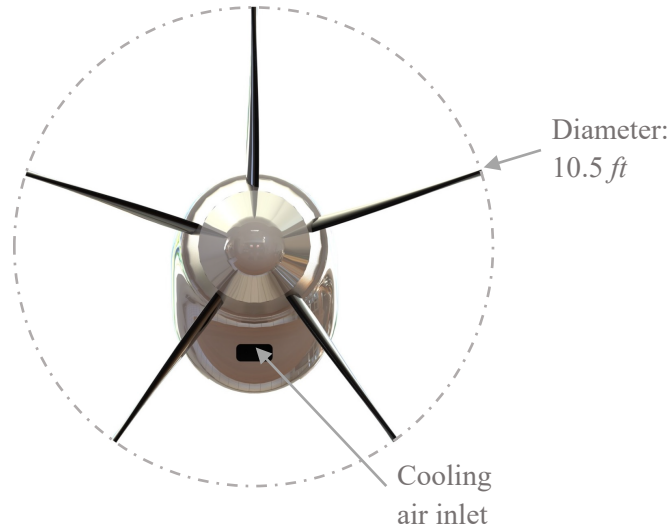


Figure 28. Five-blade propeller front view.

8 Landing Gear

8.1 Landing Gear System and Configuration

Our plane has a cruise speed of 333.6 *knots*. Therefore, a retractable landing gear is certainly more appropriate to avoid a drag penalty. Based on our plane geometry, a tricycle landing gear layout is preferred.

8.2 Preliminary landing gear and strut disposition

Although our plane only has an MTOW of 16943 *lb*, to ensure safety in case of flat tire, we choose two main wheel per strut. According to Figure 1, our main landing gear is behind the aft c.g. location. Both our nose gear and main gear position is designed to satisfy all FAR requirements as shown in Table 5 below.

	Requirement	Performance
Rotation angle	> 10°	18.4°
Tipback angle	> Rotation angle	22.9° (>18.4°)
Tipover angle	> 5°	21.3°
Overtake angle	< 60°	36.1°

Table 5. Landing gear position satisfies all FAR requirements.

8.3 Tire Sizing

Using the methods in Raymer (2012), we can determine the loading on the landing gears. Based on our aircraft drawings, $N_a = 11.7 \text{ ft}$, $M_f = 2.46 \text{ ft}$, $M_a = 2.30 \text{ ft}$ and $B = 14 \text{ ft}$. From Table 1, our maximum takeoff weight is 16943lb. Thus the Max Static Load is calculated as

$$\text{Max Static Load} = W \frac{N_a}{B} = 16943 \text{ lb} \times \frac{11.7 \text{ ft}}{14 \text{ ft}} = 14159.5 \text{ lb}$$

Since our M_a/B is 0.164, which is greater than 0.05 and our M_f/B is 0.176, which is less than 0.20, our nose gear can support this loading. Since our main landing gear has a total of four wheels, using the safety factor of 7% and 25% for further growth recommended in FAR 23, we can obtain the loads per main wheel as

$$\text{Main wheel load} = 1.07 \times 1.25 \times \frac{\text{Max Static Load}}{\# \text{ of wheels}} = 4734.58 \frac{\text{lb}}{\text{wheel}}$$

Then we can calculate our wheel diameter and width based on the equation in Table 15 as

$A \times \text{Main wheel load}^B$, where A and B is related to the aircraft type. Since our airplane is close to the business twin, our A and B are 2.69 and 0.251 for the diameter and 1.170 and 0.216 for the width. So the minimum diameter of our main gear is estimated as

$$\text{Diameter}_{\min} = 2.69 \times 4734.58^{0.251} = 22.5 \text{ in} = 1.875 \text{ ft}$$

And the minimum width of our main wheel is

$$\text{Width}_{\min} = 1.17 \times 4734.58^{0.216} = 7.28 \text{ in} = 0.6 \text{ ft}$$

Thus we choose our main gear diameter to be 1.89 ft and our main gear width to be 0.67 ft, which are both greater than the limitation. We assume our nose gear diameter is about 70% of our main gear, which is 1.34 ft. To make sure the brakes can absorb kinetic energy of aircraft, we calculate the kinetic energy during breaking as

$$\text{KE}_{\text{braking}} = \frac{1}{2} \frac{W_{\text{landing}}}{g} V_{\text{stall}}^2 \frac{1}{\# \text{ of wheels}} = \frac{1}{2} \times \frac{14159.5}{32.176} \times 135.02^2 \times \frac{1}{5} = 0.803 \times 10^6 \frac{\text{ft} \cdot \text{lb}}{\text{s}}$$

As we can see from Raymer (2012, Fig. 11.8), the chosen wheel diameter is more than the required diameter for the purpose of radiating heat. Therefore, the wheels satisfy the requirements.

8.4 Retraction Kinematics

According to Figure 29 below, our landing gear can be stored perfectly in the fuselage and nacelle.

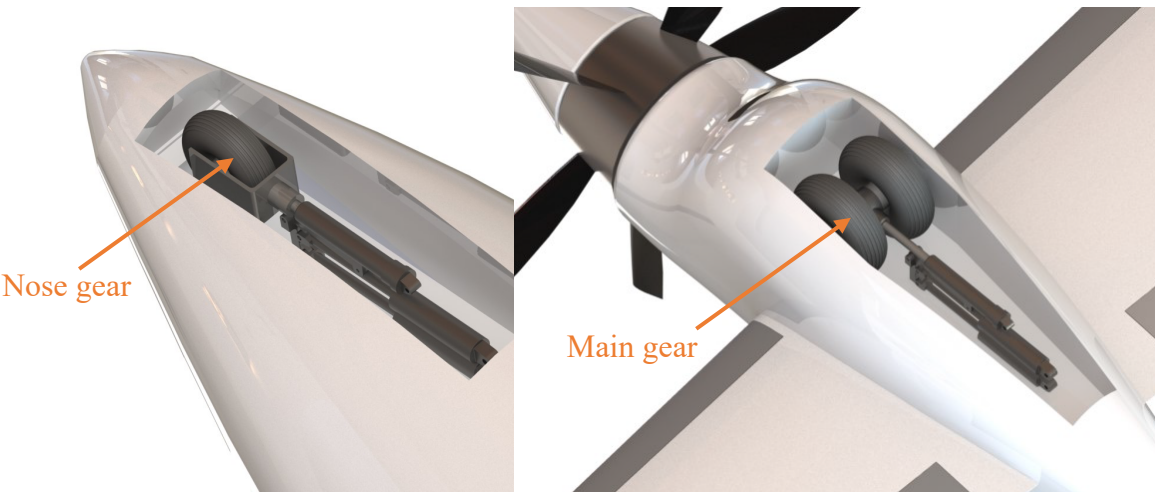


Figure 29. Landing gears can be stored perfectly in the nacelle.

Our gear linkage has a total of two degree of freedom. It has two hydraulic poles at the top, which can make sure our gear will be put down safely even if one of them is broken. The other hydraulic pole at the bottom can change the length of the rod, which not only helps to store the wheel, but also can change the height of our fuselage as mentioned in section 3.5. Since our nose gear only has one wheel, it has to turn a certain angle to be retracted into our fuselage. The detailed linkage system of our main gear and nose gear is shown in Figure 30 and Figure 31 below.

Diameter: 1.89 ft

Width: 0.67 ft

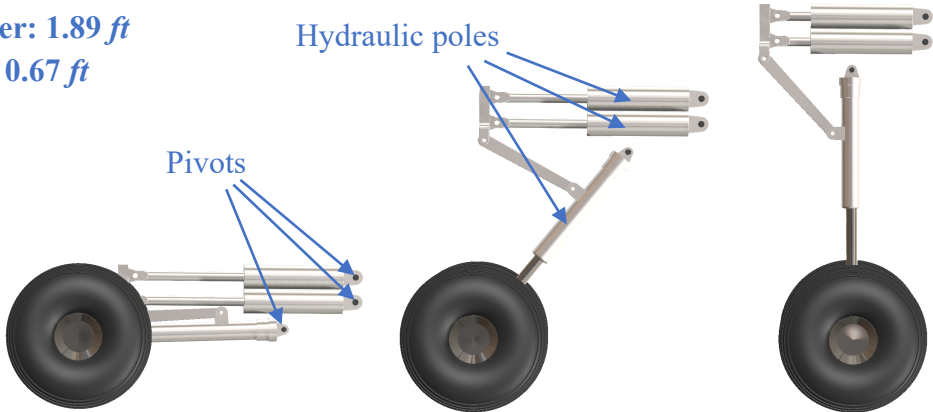


Figure 30. Main gear linkages.

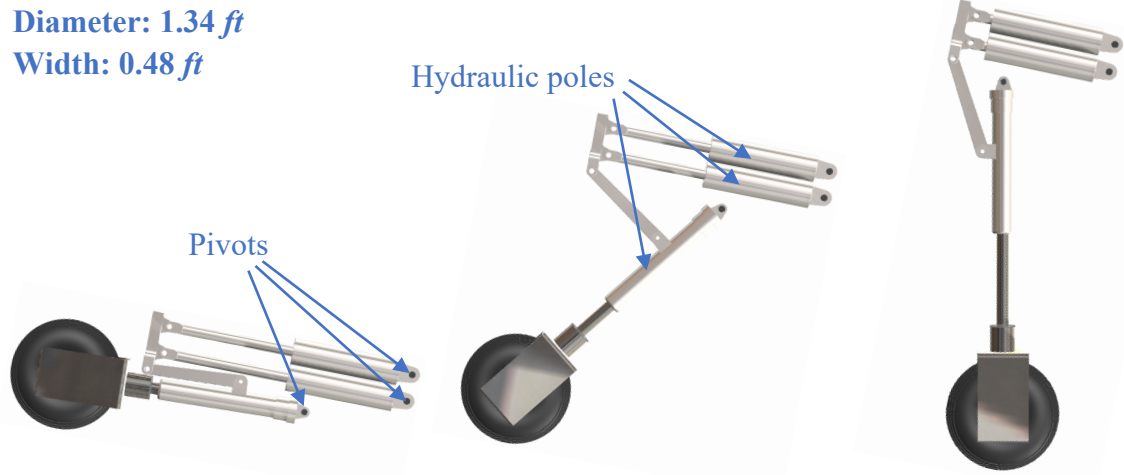


Figure 31. Nose gear linkages.

9 Method Validation

Here we validate our code by comparing the result of applying our code to King Air 350ER with King Air 350ER's actual specifications. The weight estimations for King Air 350ER are listed in the table below.

	Calculated Result	Actual King Air 350ER	Percentage Difference
MTOW [lbs]	16810	16500	1.9%
Empty Weight [lbs]	9812	9300	5.5%
Fuel Weight [lbs]	5628	5192	8.4%

Table 6. Weight validation for King Air 350ER.

From the table above, the differences between the estimated weights and King Air 350ER's actual weights are within 10% error. This means our code is valid for weight estimation. In the figure below, we plot the King Air 350ER in P-S diagram for its maximum range mission. The King Air 350ER point lies in the feasible region, which means the P-S plot is valid.

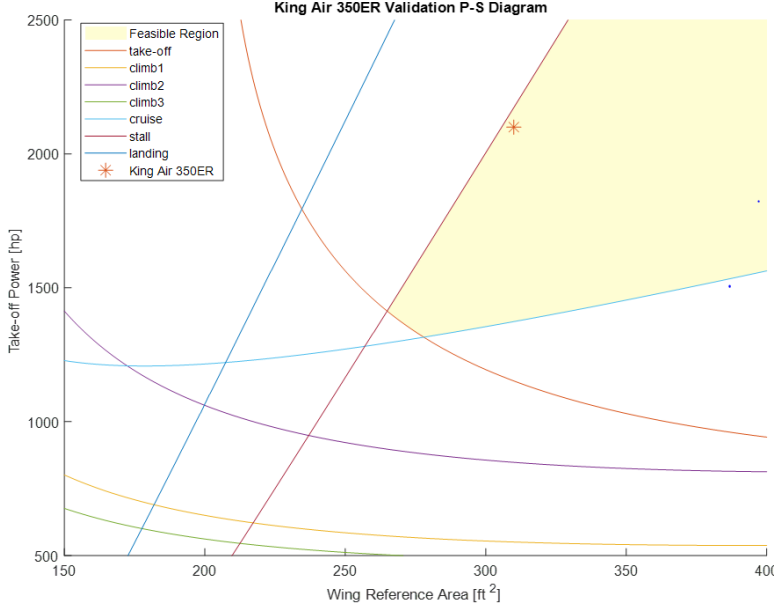


Figure 32. P-S plot validation for King Air 350ER.

We also validate our code for Ben's all-electric clean sheet.

	Calculated Result	Ben's all-electric clean sheet	Percentage Difference
MTOW [lbs]	15288	15700	-2.6%
Empty Weight [lbs]	7710	7800	-1.2%
Battery Weight [lbs]	5603	5900	-5.0%

Table 7 Weight validation for Ben's all-electric clean sheet.
Ben All-electric clean sheet Validation P-S Diagram

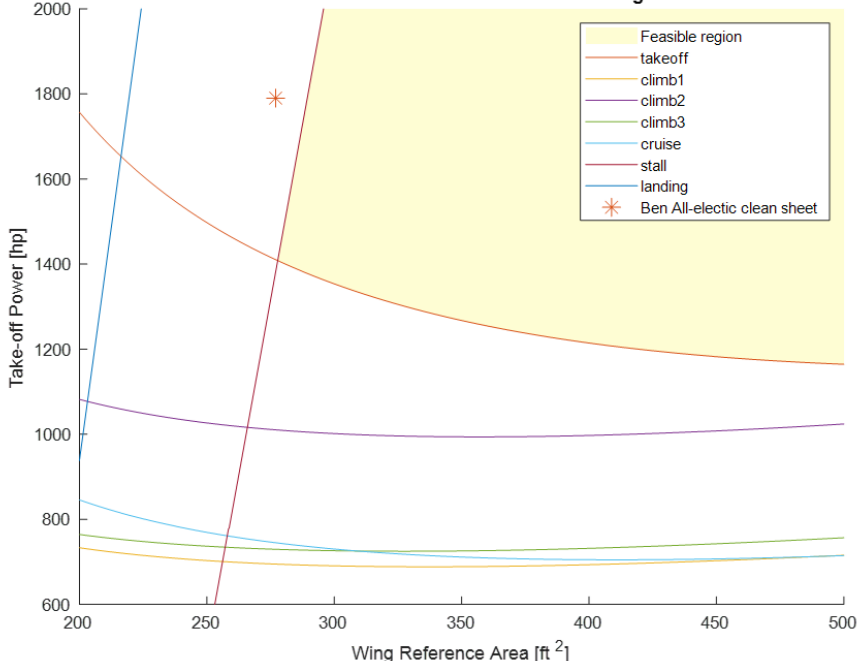


Figure 33. P-S plot validation for Ben's all-electric clean sheet.

From the Table 7 above, the differences between the estimated weights and Ben's estimates are within 5% error. This validates our weight estimate for electric airplane. However, Ben's all-electric clean sheet cannot satisfy our constraint for stall, which means maybe we have a too conservative $C_{L_{max}}$ estimation for stall condition. It satisfies all other constraint except the stall condition.

10 Objective Function

Our objective function is to minimize the direct operating cost and meanwhile satisfying FAR 23. The detailed process and results are discussed in Section 11 Design Refinement and Section 14 Cost. The minimum direct operating cost for our final electric design is 0.29 \$/nmi/pax, which is lower than our PDR design DOC of 0.38 \$/nmi/pax. We also take environmental issues and noise issues into account. Since electric configuration is more environmentally friendly and produces less noise. Thus, we choose electric design for the mission.

11 Design Refinement

The direct operating cost is significantly influenced by our aircraft sizing and flight performances. We introduce eight independent variables to refine our design: cruise speed, altitude, climb angle, descent angle, aspect ratio, taper ratio, wing incidence angle and twist angle. We use gradient based optimization method to minimize DOC by finding the optimal design variable values. We have integrated AVL into our loop for induced drag and trim drag calculation, and update the wing and empennage design for the AVL geometry model every loop. Then we calculate the DOC gradient with respect to eight different variables and choose the opposite direction to be our optimization direction. Here is the figure (Figure 34) shows our iterations. The initial guesses of our design are 238 knots cruise speed, 25000 ft altitude, 8° climb angle, 3° descent angle, 12 aspect ratio, 0.5 taper ratio, 3° incidence angle and -3° twist angle. The optimal point has 333.6 knots cruise speed, 32200 ft altitude, 10° climb angle, 6° descent angle, 12.67 aspect ratio, 0.454 taper ratio, 2.9° incidence angle and -1.6° twist angle.

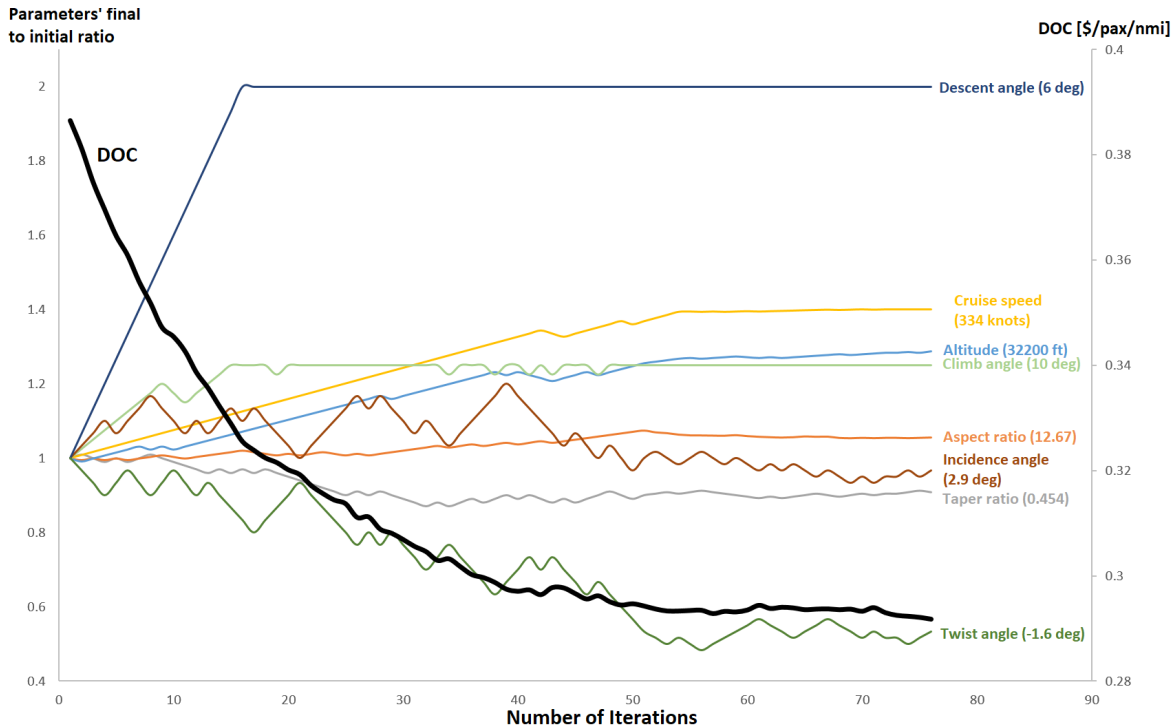


Figure 34. The result converges after about 80 iterations.

After we figure out the optimal design point, we can do trade study based on that point.

11.1 Cruise Speed Trade Study

DOC is a function of block time and block time mainly depends on cruise speed. So cruise speed has a large influence on DOC. Figure 35 shows the relationship of cruise speed, MTOW and DOC. Although MTOW increases when cruise speed increases, DOC is still decreasing before 333.6 knots. In order to minimize DOC, we choose cruise speed of 333.6 knots. This is about Mach 0.57 at 32200 ft altitude, which is still subsonic. We do not have trouble with transonic compressibility effects.

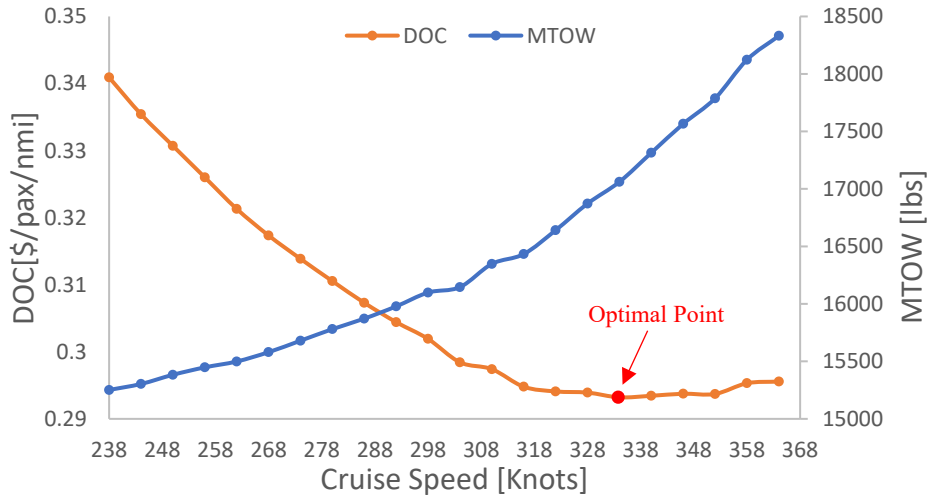


Figure 35. Cruise speed of 333.6 knots has the lowest DOC.

11.2 Altitude Trade Study

Altitude is another flight parameter which influences DOC. A high altitude has a low density, thus a low drag. But a high altitude also needs longer climb and descent time. We plot the relationship of altitude, MTOW and DOC in Figure 36. We can see altitude of 32200 ft has minimum DOC. From the trend on the plot, we can see MTOW keeps decreasing as altitude goes up, but the longer block time makes DOC increase after 32200 ft.

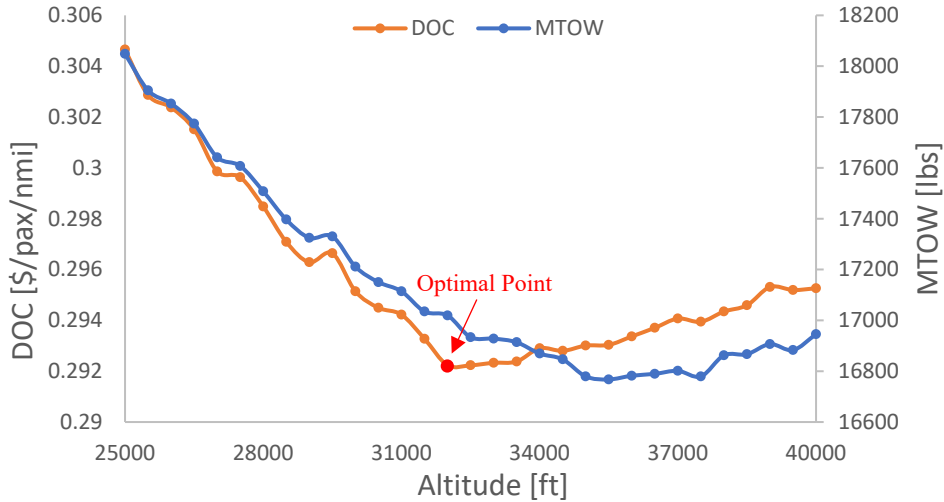


Figure 36. Altitude of 32200 ft has a minimum DOC.

11.3 Climb and Descent Angles Trade Study

During the flight, climb and descent angles determine the block time and energy consumption. We want to optimize climb and descent angles to minimize DOC. From the plot below (Figure 37 and Figure 38),

we can see that DOC decreases as the climb and descent angles increase. However, since we need to consider the comfortability of passengers, we do not want too steep climb and descent stages. Thus, we choose 10 degrees for climb and 6 degrees for descent.

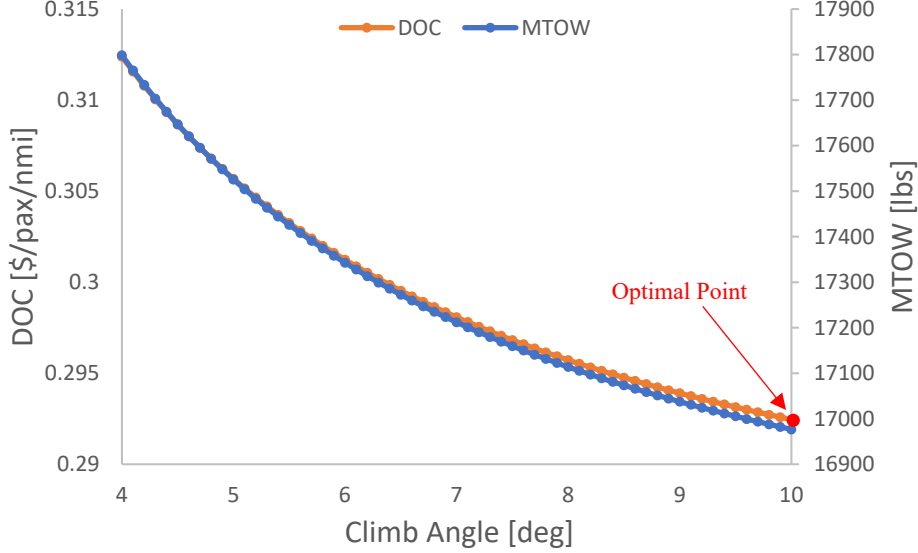


Figure 37. Climb angle should be as large as possible for a low DOC.

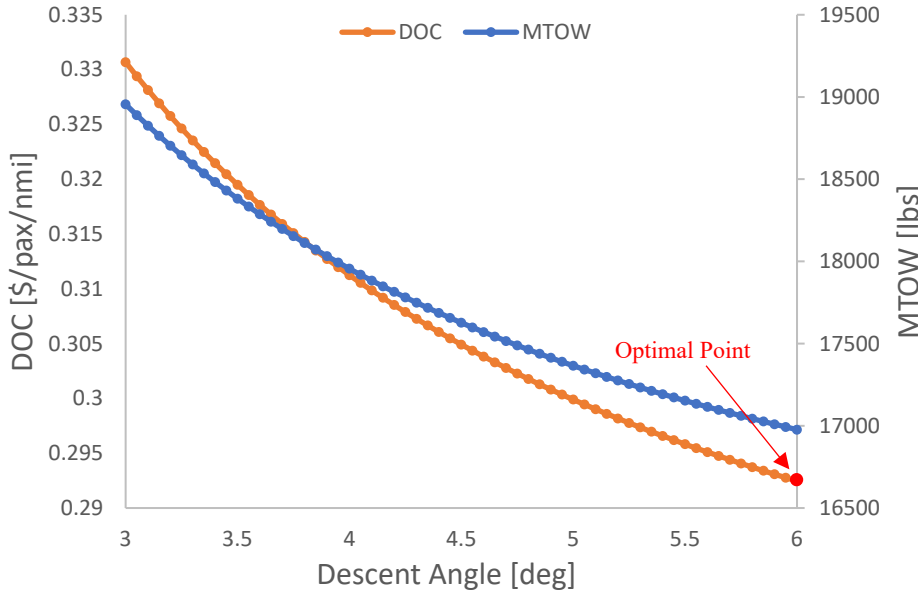


Figure 38. Descent angle should be as large as possible for a low DOC.

11.4 Aspect Ratio Trade Study

Aspect ratio is a wing design parameter which relates to induced drag and wing structure weight. According to the wing induced drag equation:

$$C_{D_i} = \frac{c_L^2}{\pi AR e},$$

A high aspect ratio wing will have a low induced drag. However, according to Raymer and Kroo's wing weight estimation equations, the wing structure weight increases as aspect ratio increases. So there is a tradeoff between weight and drag due to aspect ratio changes. We plot the relationship of aspect ratio, MTOW and DOC in Figure 39. Here we find for AR from 10 to 13, DOC and MTOW are always decreasing with respect to an increasing aspect ratio. But we need to consider some constraints for the

maximum span. For a similar mission airport, for example the Ann Arbor airport, the runway width is only 75 ft. In order to avoid any accident on the runway, we limit the maximum span to be 65 ft. Therefore, aspect ratio 12.67 is calculated to be our optimal aspect ratio.

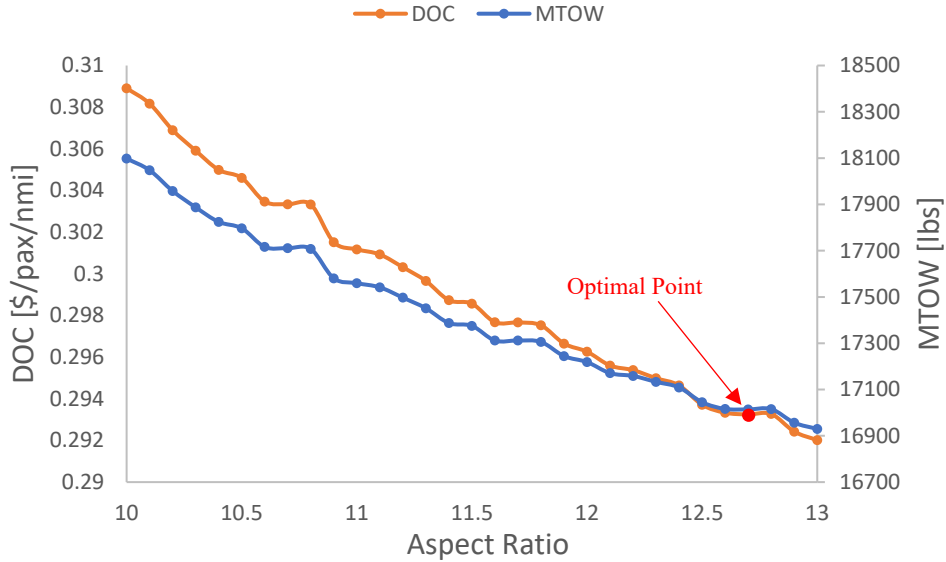


Figure 39. Aspect ratio 12.67 is selected for a limited span width.

11.5 Taper Ratio Trade Study

Taper ratio affects wing structure weight and wing lift distribution. To get a good lift distribution for a low drag, and to minimize wing weight, we plot the relationship of taper ratio, MTOW and DOC in Figure 40. Here we find the lowest DOC occurs at taper ratio around 0.4 to 0.5. Our optimization gives us the local minimum at 0.454.

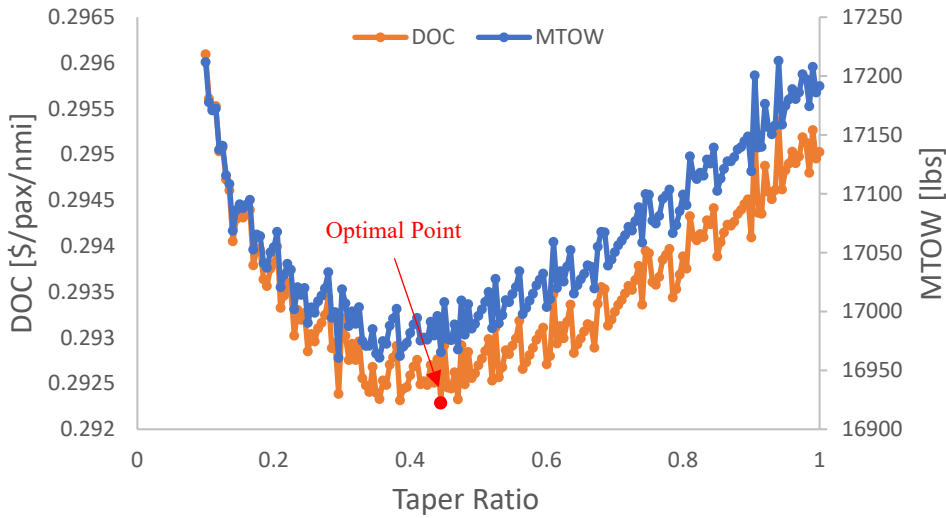


Figure 40. Taper ratio 0.454 is optimal for a low DOC.

11.6 Incidence and Twist Angles Trade Study

The incidence of the wing and twist of the wing tip also affect the lift distribution and drag. However, these two variables don't have a large impact on DOC. We use AVL to analyze the effects of changing incidence and twist, but the result is quite noisy. We believe AVL's vortex panel method is not so

sensitive to small incidence and twist changes. Also, our model doesn't have a large span-wise panels so the results are not accurate. But we can still see some trends from Figure 41 and Figure 42. The minimum DOC occurs at 2.9° incidence angle and -1.6° twist angle.

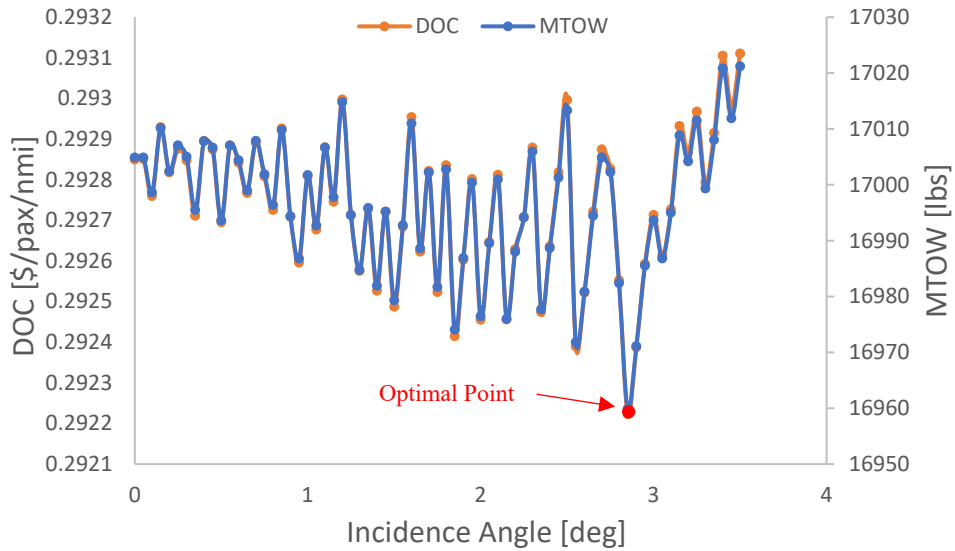


Figure 41. Minimum DOC occurs at incidence angle of 2.9 degrees.

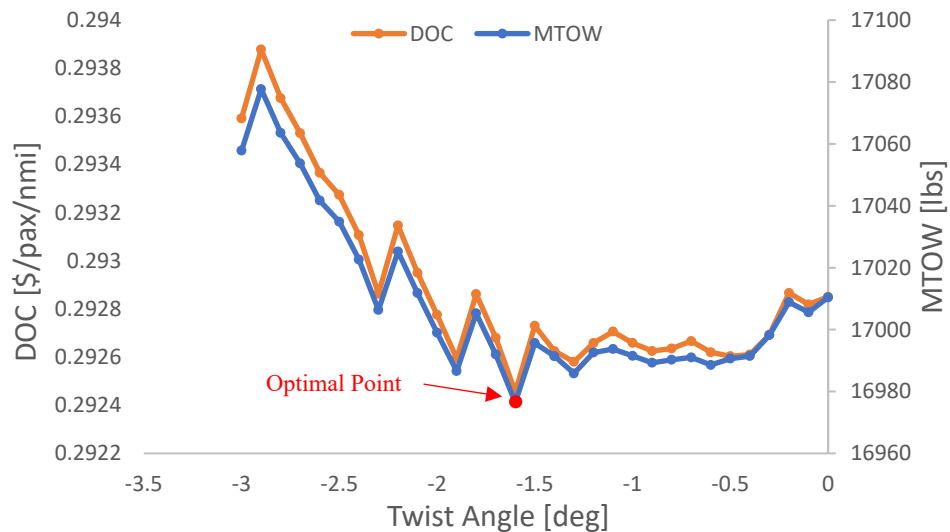


Figure 42. Minimum DOC occurs at twist angle of -1.6 degrees.

12 Final Sizing

12.1 P-S Diagram

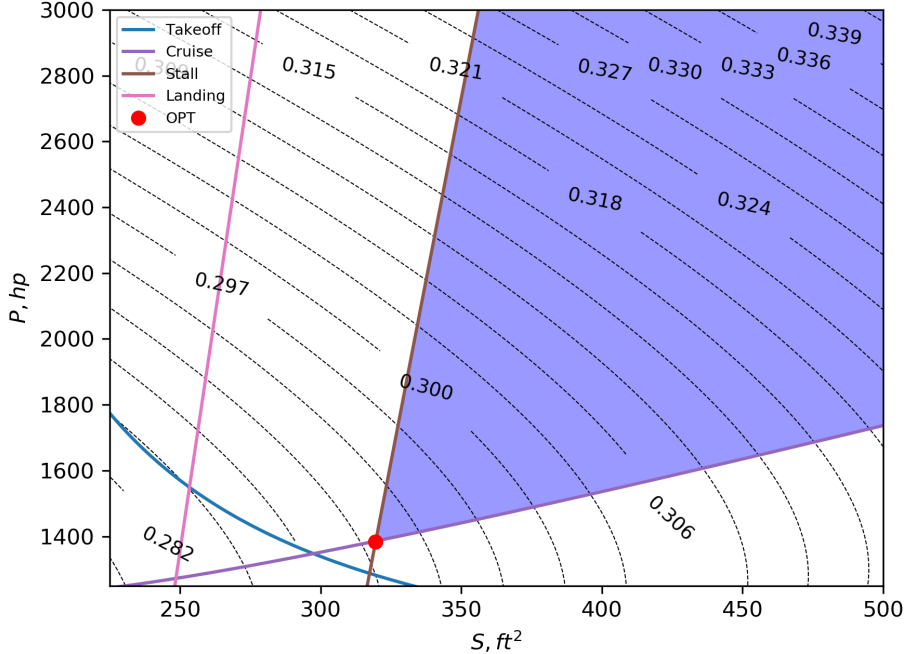


Figure 43. P-S Diagram with DOC contour.

Based on our improved weight estimate, we reconsider the constraints from each flight segment. The P-S diagram shows the relationship between direct operating cost with different power and surface area with one set of other design variables, which includes the aspect ratio AR , taper ratio λ , cruise speed V_{cr} , climb angle, descent angle, twist and incidence angle. Using the P-S diagram, we can determine the optimal point for each set of design variable. Figure 43 shows the P-S diagram determining the final design variables, which leads to a DOC of $0.29 \$/nmi/pax$. The blue region is the feasible region and the black dashed line is the DOC contour. By using the optimization process, we effectively decreased the DOC by approximately 25%.

On the figure shown above, the optimal point is constrained by the cruise constraint and the stall constraint. From the trade study, we have found that for relatively low cruise speed, the optimal point is constrained by takeoff and stall while for relatively high cruise speed, the optimal point is constrained by cruise and stall.

12.2 Refinement Comparison Table

Since we have improved our design from PDR, we can compare the design parameters between PDR and CDR. The comparison Table 8 is shown below. We have a similar takeoff weight and wing reference area, a slightly lower power, but a much faster cruise speed. With a 333.6 knots cruise speed, although we are flying at a lower L/D compared with PDR design, our CDR design still has a much lower DOC.

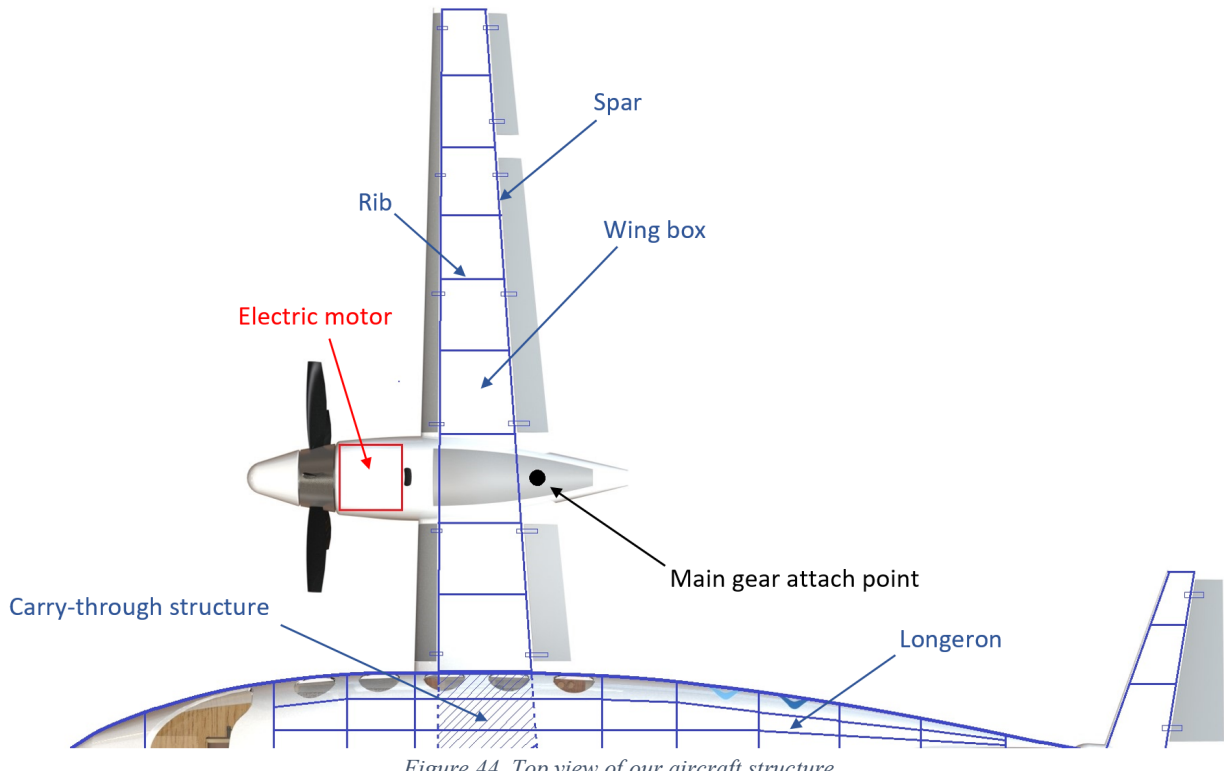
	PDR	CDR	difference
MTOW [lbs]	17056	16943	-0.7%
Empty Weight [lbs]	8402	8817	4.9%
Battery Weight [lbs]	6679	6150	-7.9%
Power [hp]	1600	1502	-6.1%
Wing Area [lbs]	330	330	0.0%
Altitude [ft]	30000	32200	7.3%
Cruise Speed [knot]	238	333.6	40.2%
Aspect Ratio	10	12.67	26.7%
Taper Ratio	0.5	0.454	-9.2%
Incidence Angle [deg]	3	2.9	-3.3%
Twist Angle [deg]	-3	-1.6	-46.7%
Cruise L/D	16.3	14.4	-11.7%
DOC [\$/pax/nmi]	0.38	0.29	-23.7%

Table 8. CDR improved design has a lower DOC compared with PDR design.

13 Structure

13.1 Load paths

Our aircraft structure is shown in Figure 44 and Figure 45. There are two spars in our wing box, and 10 ribs in a half wing. The fuselage has formers and longerons to support the structure. Vertical tail and horizontal tail are also containing two spars and few ribs.



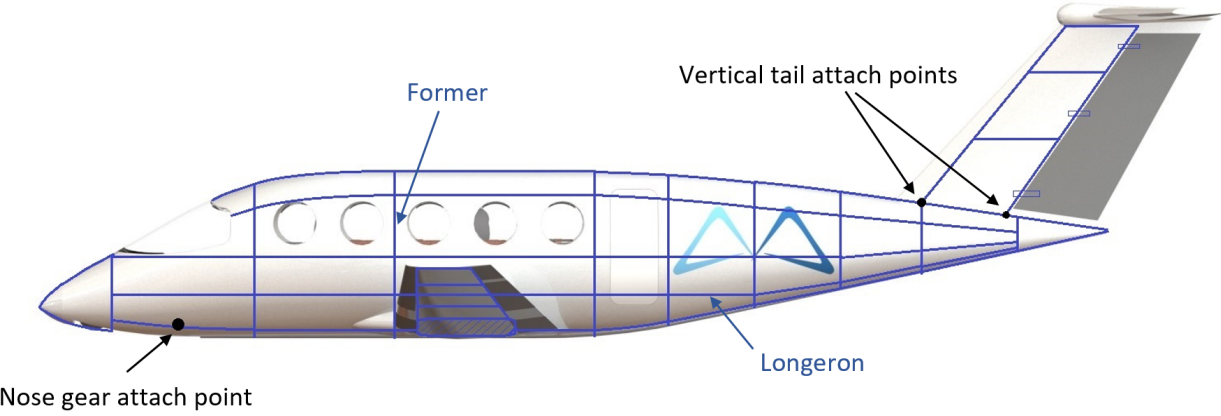


Figure 45. Side view of our aircraft structure.

13.2 V-n diagram

We first calculate the maneuver envelope that shows the equivalent airspeed and load factor limit. The constraints are given by following equations:

$$n = \frac{L}{W} = \frac{\rho_{SL} V_{EAS}^2 C_{L_{max}}}{2W/S}$$

$$n_{limit} = 2.1 + \frac{24000}{W + 10000}$$

Where V_{EAS} is the equivalent airspeed at sea level, $C_{L_{max}} = 1.62$ and $C_{L_{max_neg}} = -1.60$ at cruise when Reynolds number is 9000000. Then we add the gust envelope onto V-n diagram. The gust line equation is:

$$n = 1 \pm \frac{K_g C_{L_\alpha} U_e V_{EAS}}{498W/S}$$

Where detailed equations for K_g and C_{L_α} are listed in 18.3.4. The U_e is the equivalent gust velocity in ft/sec, which can be linearly interpolated when cruise height is between 20000 ft and 50000 ft. The values are shown in Table 9.

	Altitude 20000 ft and below (ft/s)	Altitude 50000 ft and above (ft/s)
U_{eB} (rough air gust)	66	38
U_{eC} (gust at max design speed)	50	25
U_{eD} (gust at max dive speed)	25	12.5

Table 9. Equivalent gust velocity at different cruise height.

The V-n diagrams for maximum weight and minimum weight at cruise height 20000 ft and 32200 ft are shown below:

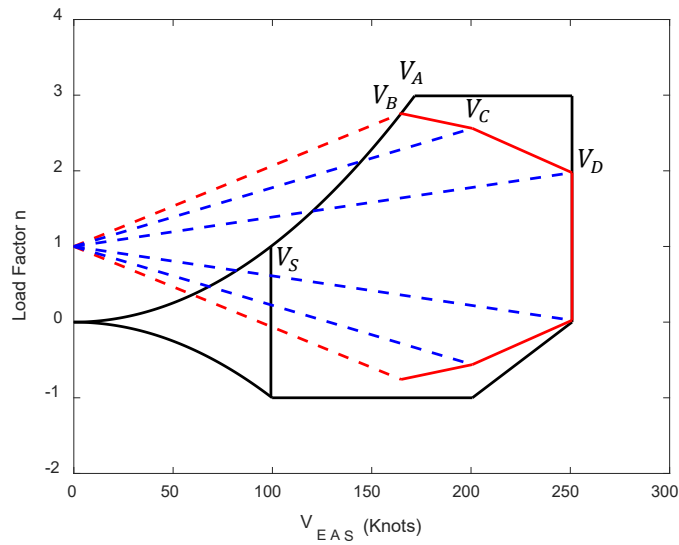


Figure 46. V - n diagram at designed cruise height 32200 ft and maximum weight 16943 lb.

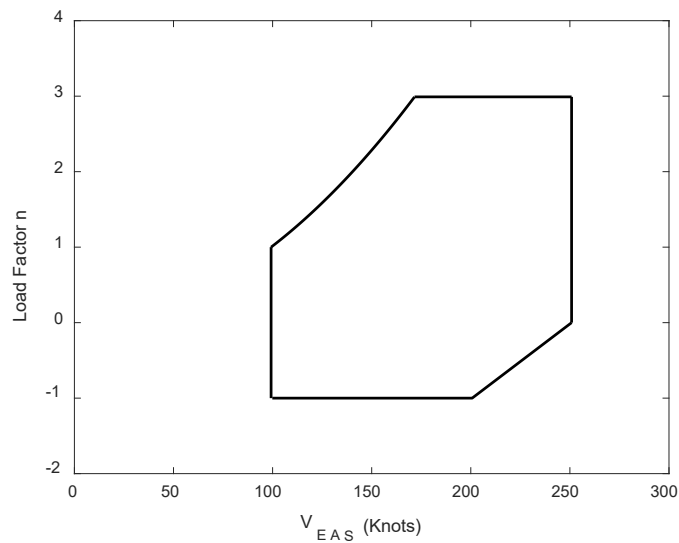


Figure 47. Final envelope at designed cruise height 32200 ft and maximum weight 16943 lb.

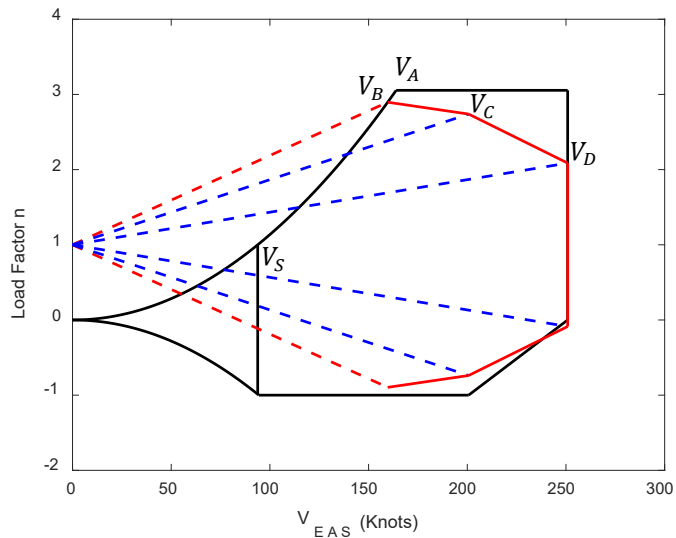


Figure 48. V - n diagram at designed cruise height 32200 ft and minimum weight 15143 lb.

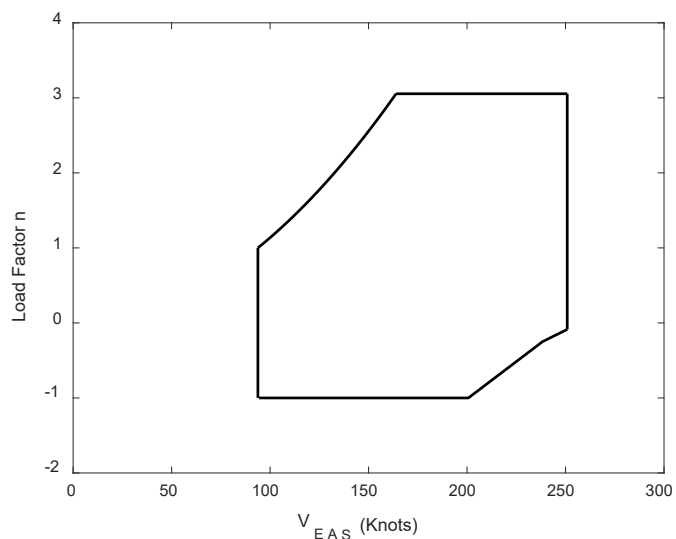


Figure 49. Final envelope at designed cruise height 32200 ft and minimum weight 15143 lb.

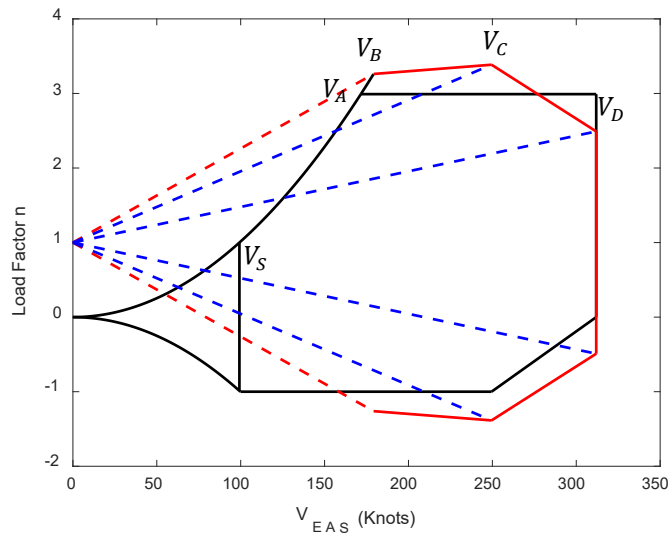


Figure 50. $V\text{-}n$ diagram at worst gust condition cruise height 20000 ft and maximum weight 16943 lb.

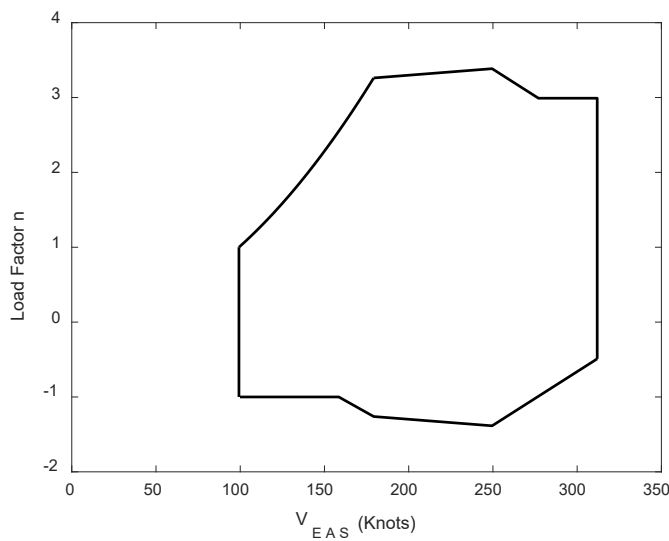


Figure 51. Final envelope at worst gust condition cruise height 20000 ft and maximum weight 16943 lb.

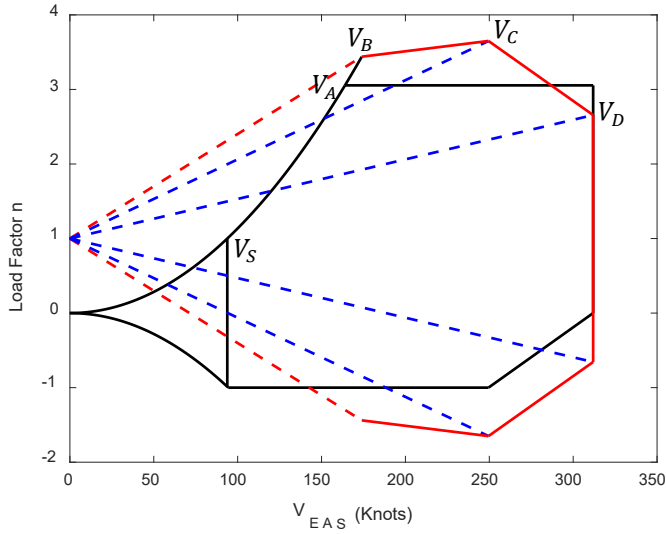


Figure 52. $V\text{-}n$ diagram at worst gust condition cruise height 20000 ft and minimum weight 15143 lb.

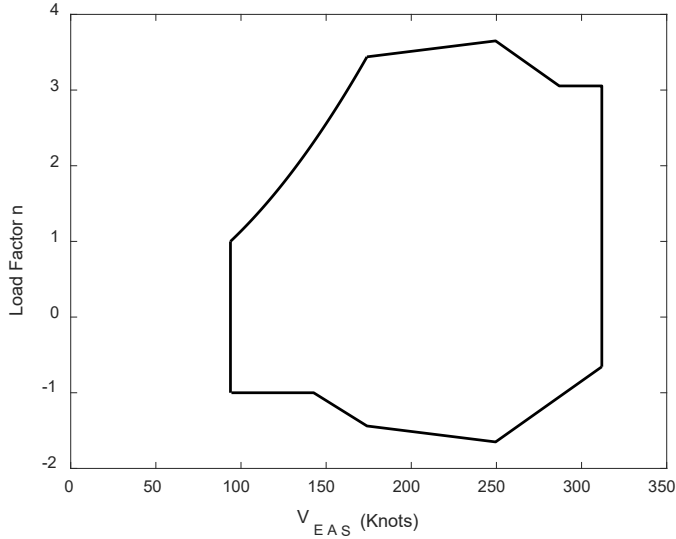


Figure 53. Final envelope at worst gust condition cruise height 20000 ft and minimum weight 15143 lb.

As shown in the $V\text{-}n$ diagrams, when the cruise height is 32200 ft, the load limits are constrained by maneuver envelope, and when cruise height is 20000 ft, which is worst gust condition, the load limits are mostly constrained by gust envelope.

13.3 Distribution of Air Loads on the Wing

The distributions of air loads on the wing in cruise, takeoff and landing are simulated by AVL and the results are shown in Figure 21, Figure 20 and Figure 19.

14 Cost

The main objective of our mission is to minimize direct operating cost (DOC), which is the sum of cash operating cost (COC) and fixed operating cost (FOC). We can calculate each component of DOC directly after we determine our final design. The DOC table for our final design is shown below (Table 10). The flight stages and block time breakdown are shown in Figure 55.

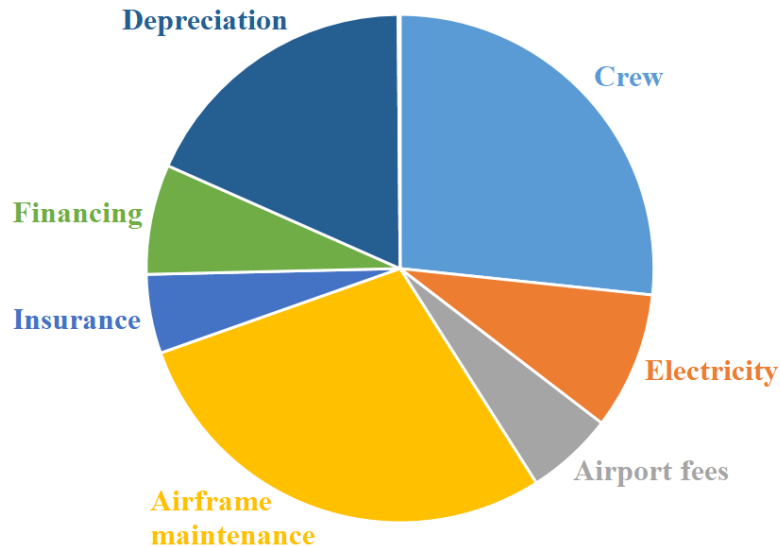


Figure 54. Pie chart for DOC.

	Cost (Year 2030 USD)
Crew	244
Attendants	0
Electricity	80
Airport fees	51
Navigation fees	0
Airframe maintenance	262
Motors maintenance	neglect
COC	638
COC/pax-nmi	0.20
Insurance	46
Financing	64
Depreciation	167
Registration	1.1
DOC	919
DOC/pax-nmi	0.29
Aircraft price	7.34 million

Table 10. DOC breakdown.

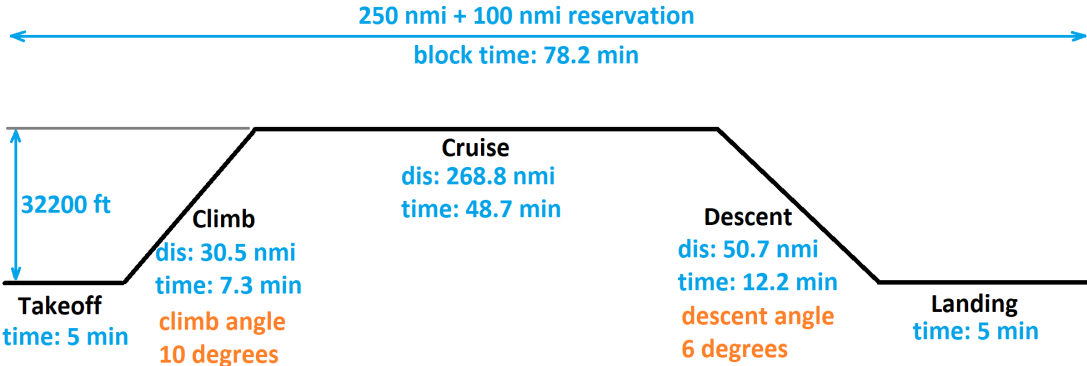


Figure 55. Flight stages and block time breakdown.

15 Computation Procedure

15.1 Optimization Process

To further decrease the direct operating cost, we setup eight independent design variables, which includes aspect ratio AR , taper ratio λ , cruise speed V_{cr} , cruise altitude h , climb angle, descent angle, twist and incidence angle. Figure 56 shows the flow chart for the optimization process.

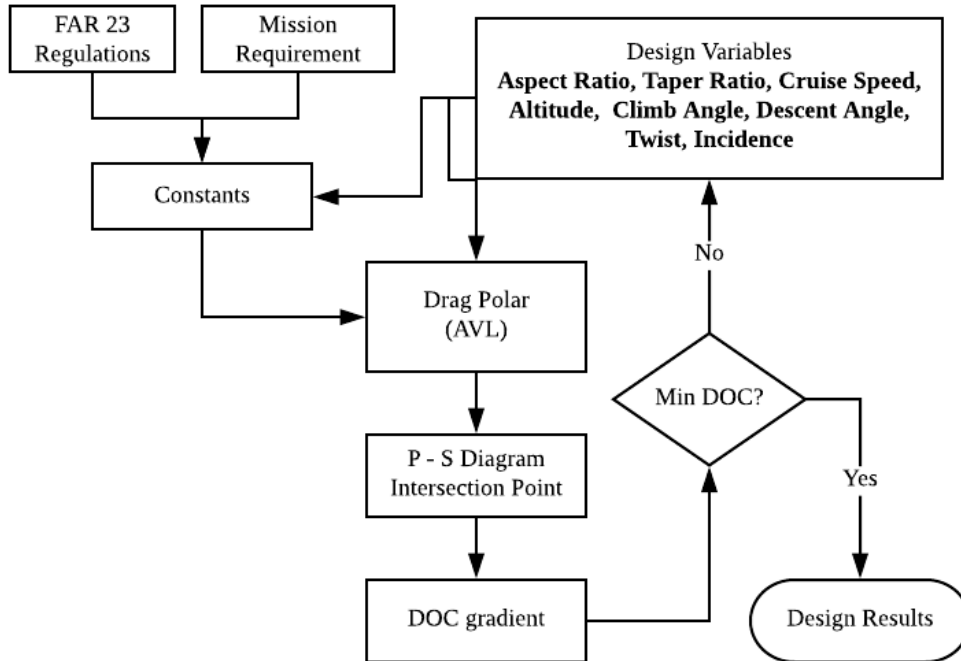


Figure 56 Optimization Process.

With mission requirements and regulations input, some related global constants such as Mach number for cruise, climb, takeoff and landing are calculated for further use. Then one set of design variables is setup for the calculation for drag polar using AVL results. By finding the optimal point on the P-S diagram, which is constrained by the regulations on cruise, stall, landing, takeoff and three climb stages, the direct operating cost is calculated for the particular point. The gradient of the DOC is calculated and it determines the direction of the minimum DOC direction. The optimization iteration goes on until a final acceptable minimized DOC is determined.

15.2 Improved Estimation

Compared to the preliminary design stage, the DOC is decreased by 25% effectively after the optimization process. Apart from more accurate lift and drag coefficient relationship, parasitic drag for different stages is calculated, accounting for a part of the drag coefficient which cannot be calculated by AVL. Configurations for high lift device introduces increase in lift and drag coefficient, which are also accounted for based on specific geometry with variables such as flapped area, flap/slat deflection angles, which are more accurate than historical values used during the preliminary design.

AVL analysis for clean sheet configuration is introduced into each loop of iteration. Since AVL needs complete definition of the wing geometry, whenever any variables related to wing geometry changes, such as reference area, AVL is used to recalculate a more accurate drag polar. Therefore, the consequent calculation for weight and power estimation can be more accurate based on the updated drag polar.

15.3 Python Module Breakdown

For preliminary design, we used MATLAB for calculation while after we decided to integrate AVL into iteration loop, we changed language to python so that the optimization process is less time-consuming. The following part shows how the functions within the software are used and interact with each other.

opt.py: calculate optimization results

constants.py: calculate and store constants for optimization process

requirements.py: store mission requirements

dragpolar.py: calculate drag polar coefficients [a,b,c] for six configurations

```
dragpolar (P, S, CL,max, dragpolar, Plot = False):
    return dragpolar
```

AVL.py: interactions with AVL executable

```
write (M, S, AR, λ, fuselage = False, flaps = False):
    # write .avl file with specified aircraft geometry
    return zero
run (αi, αf, flap = 0, slat = 0):
    # interact with AVL executable and record CL and CD calculation results
    # αi, αf are the start and the end of the angle of attack sequence for calculations
    return 0
read():
    # read output files of AVL, extract lift and drag coefficients, return curve-fitting
    # coefficients [a, b, c]
    return [a ,b, c]
```

battery_fraction.py: calculate battery fraction for a certain set of design variables

```
battery_fraction (R, AR, W, P, S, dragpolar):
    return  $\frac{W_{battery}}{W_{TO}}$ 
```

DOC_calc.py: calculate direct operating cost

```
DOC_calc (P, W, S, dragpolar):
    return DOC
```

MTOW.py: calculate estimations for maximum takeoff weight

```

MTOW ( $P, S, dragpolar$ ):
    return  $MTOW$ 

```

parasitedrag.py: calculate C_{D0} for six configurations on the drag polar

```
parasitedrag( $S, stage$ ):
```

```

# stage are numbered as 1. takeoff gear down flap down; 2. takeoff gear up flap down; 3.
# landing gear down flap down; 4. landing gear up flap down; 5. climb & descent; 6.
# cruise
return  $C_{D0}$ 

```

PS.py: calculate six constraints for (P, S) and decide the optimal point

```
PS ():
```

```

# constants are stored in the constants.py, no further inputs are needed
return  $S_{opt}, P_{opt}, W_{opt}, DOC$ 

```

15.4 Python Module Interaction

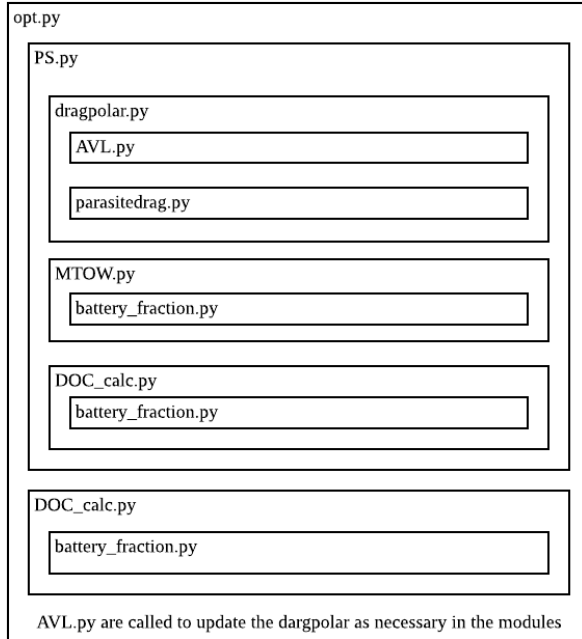


Figure 57. Python Modules.

From Figure 57, the interactions between different modules are shown. Note that *AVL.py* are used for updated drag polar whenever necessary during the optimization process to ensure accuracy.

16 Conclusions

Air Infinity presents the critical design of an electric commuter airplane which is capable to fly at economic range of 250 *nmi* and maximum range of 400 *nmi* with 100 *nmi* reserve. The critical design meets all flight requirements. It can carry 9 passengers and 1 pilot. The baggage cabinet volume for our electric aircraft is 30 ft^3 , which satisfies well with the baggage requirement of nine 25-*lbs* baggage.

Our electric airplane has a single fuselage, a low wing, two electric motors mounted on the wing, a T-tail and a tricycle landing gear configuration.

After the optimization, our final design has a MTOW of 16943 *lb* and uses two Magni500 motors to provide total rated power of 1502 *hp*. The fuselage length is 45 *ft* and fuselage diameter is 7 *ft*. The wing has a reference area of 330 ft^2 , with an aspect ratio of 12.67, a taper ratio of 0.454, zero sweep, 6° dihedral angle, 2.9° incidence angle and -1.6° twist angle. The cruise altitude is 32200 *ft* and the cruise speed is 333.6 *knots*. The static margin is 9.8% and the direct operating cost per passenger per *nmi* is 0.29.

Comparing with similar size existing airplanes, our Air Infinity electric airplane has a relatively fast cruise speed, which is a main factor to reduce direct operating cost. For the mission around Pacific Northwest region, our electric airplane has a lower direct operating cost than conventional turboprop airplanes. In addition, electric airplane has much lower noise and lower carbon dioxide emission. These advantages let us recommend our electric airplane design for the mission.

17 References

- [1] Daniel P. Raymer. Aircraft Design: A Conceptual Approach. AIAA, 5th edition, 2012.
- [2] <https://www.magnix.aero/products/>
- [3] Joaquim R. R. A. Martins, The Metabook of Aircraft Design, Canvas
- [4] Raymer, D. P. (1989) *Aircraft Design: A Conceptual Approach*. Washington, D.C.: American Institute of Aeronautics and Astronautics, Inc.

18 Appendix

18.1 List of Symbols

Symbols	Explanation
C_L	Aircraft lift coefficient
$C_{L,max}$	Maximum lift coefficient
C_D	Aircraft drag coefficient
C_{D_0}	Parasite drag coefficient
C_l	Sectional lift coefficient
C_d	Sectional drag coefficient
AR	Aspect ratio
b	Span
e	Wing loading efficiency factor
α	Angle of attack
c_{root}	Root chord
S or S_{ref}	Wing reference area
P	Power
W or $MTOW$	Maximum takeoff weight
L/D	Lift drag ratio
V	Aircraft air speed
M	Mach number
DOC	Direct operating cost
X_{CG}	Center of gravity x position
X_{MAC}	Mean aerodynamic chord x position
X_{RLE}	Leading edge root x position
Λ	Sweep angle
λ	Taper ratio
N_Z	Ultimate Load Factor
S_{cs_w}	Wing mounted control surface area

Table 11. List of symbols.

18.2 Supplementary Drawings

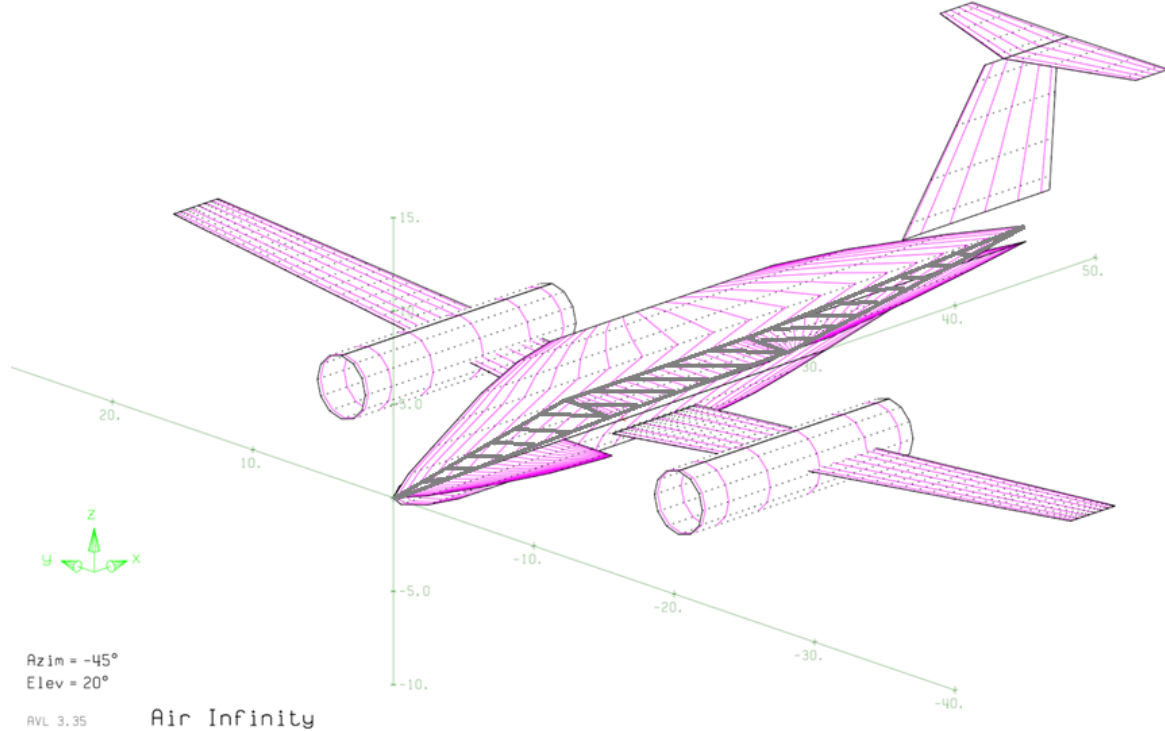


Figure 58. AVL model for our critical design.

18.3 Supplementary Equations

18.3.1 Direct Operating Cost Equation

$$b_{CEF} = 5.17053 + 0.104981(b_{year} - 2006)$$

$$t_{CEF} = 5.17053 + 0.104981(t_{year} - 2006)$$

$$CEF = \frac{t_{CEF}}{b_{CEF}}$$

$$C_{crew} = AF[K(MTOW)^{0.4}t_b](CEF)$$

AF = airline factor = Average = 0.80

K = route factor = 2.75 for regional routes

$$C_{attd} = 60n_{attd}(CEF)(t_b)$$

$$C_{fuel} = \frac{1.02W_f P_f}{\rho_f}$$

$$C_{elec} = 1.05W_b P_{elec} e_{elec}^*$$

$$C_{oil} = \frac{1.02W_{oil} P_{oil}}{\rho_{oil}}$$

$$W_{oil} = \frac{0.0125W_f t_b}{100}$$

$$C_{airport} = 1.5 \left(\frac{MTOW}{1000} \right) (CEF)$$

$$C_{aircraft} = 10^{1.1846 + 1.2625 \log_{10} MTOW} (CEF)$$

$$\begin{aligned}
C_{engines} &= 10^{2.5262+0.9465 \log_{10} SHP_{TO}}(CEF) \\
C_{airframe} &= C_{aircraft} - C_{engine} \\
C_{ML} &= 1.03 \left(3 + \frac{0.067 W_{airframe}}{1000} \right) R_L \\
C_{MM} &= 1.03(30CEF) + 0.79 \times 10^{-5} C_{airframe} \\
C_{airframe maintenance} &= (C_{ML} + C_{MM}) t_b \\
C_{MLengine} &= 1.03 \cdot 1.3 \left(0.4956 + 0.0532 \frac{\frac{SHP_{TO}}{n_{engine}}}{1000} \frac{1100}{H_{em}} + 0.1 \right) R_L \\
C_{engine maintenance} &= n_{engine}(C_{ML} + C_{MM}) t_b \\
c_{motors} &= 150/hp \\
c_{batteries} &= 520/kWh \\
C_{electric aircraft} &= C_{aircraft} - C_{engines} + C_{motors} + C_{batteries} \\
U_{annual} &= 1.5 \times 10^3 \left[3.4546 t_b + 2.994 - (12.289 t_b^2 - 5.6626 t_b + 8.964)^{0.5} \right] \\
C_{insurance} &= \left(\frac{IR_a C_{aircraft}}{U_{annual}} \right) t_b \\
C_{financing} &= 0.07 DOC \\
C_{depreciation} &= \frac{C_{unit} (1 - K_{depreciation}) t_b}{n(U_{annual})} \\
C_{registration} &= (0.001 + 10^{-8} MTOW)(DOC) \\
DOC &= C_{crew} + C_{attd} + C_{fuel} + C_{oil} + C_{airport} + C_{airframe maintenance} + C_{engine maintenance} \\
&\quad + C_{insurance} + C_{financing} + C_{depreciation} + C_{registration}
\end{aligned}$$

18.3.2 Weights and CG Location Estimates Equation

$$\begin{aligned}
W_{wing} &= 0.0051(W_0 N_z)^{0.557} S_w^{0.649} AR^{0.5} \left(\frac{t}{c} \right)_{root}^{-0.4} (1 + \lambda)^{0.1} (\cos \Lambda)^{-1} S_{cs}^{0.1} \\
W_{wing} &= 4.22 S_{wing} + 1.642 \times 10^{-6} \frac{n b^3 \sqrt{W_0^2} (1 + 2\lambda)}{S_{wing} \left(\frac{t}{c} \right) \cos^2 \Lambda (1 + \lambda)}
\end{aligned}$$

18.3.3 Stability Equation

$$\frac{x_{np}}{\bar{c}} = \frac{l_h S_h}{\bar{c} S_w} \frac{C_{L\alpha h}}{C_{L\alpha w}} - \frac{1}{C_{L\alpha w}} \frac{\partial C_{mfus}}{\partial \alpha} = 0.3742$$

$$\text{static margin} = \frac{x_{np} - x_{cg}}{\bar{c}} = 0.09794$$

$$C_{L\alpha h} = C_{L\alpha h 0} \left(1 - \frac{\partial \varepsilon}{\partial \alpha} \right) \eta_h = 2.69$$

$$C_{L\alpha} \approx \frac{2\pi AR}{2 + \sqrt{\left(\frac{AR}{\eta} \right)^2 (1 + \tan^2 \Lambda - M^2) + 4}}$$

$$\frac{\partial \varepsilon}{\partial \alpha} \approx \frac{2C_{L\alpha w}}{\pi AR_w} = 0.2966$$

$$\frac{\partial C_{mfus}}{\partial C_L} = \frac{K_f w_f^2 L_f}{S_w \bar{c} C_{L\alpha w}} = 0.09267$$

18.3.4 V-n diagram equation

$$K_g = \frac{0.88\mu}{5.3 + \mu}$$

$$\mu = \frac{2\left(\frac{W}{S}\right)}{\rho \bar{C} C_{L_\alpha} g}$$

$$C_{L_\alpha} = \frac{2\pi AR}{2 + \sqrt{AR^2 \left(\frac{\beta}{k}\right)^2 \left(1 + \frac{\tan^2 A_c}{\beta^2}\right) + 4}}$$

$$\beta = \sqrt{1 - M^2} \quad k = 0.97$$

18.4 Supplementary Tables or Figures from Textbook

Table 12.2 Approximate lift contributions of high-lift devices

High-lift device	$\Delta C_{l_{max}}$
Flaps	
Plain and split	0.9
Slotted	1.3
Fowler	1.3 c'/c
Double slotted	1.6 c'/c
Triple slotted	1.9 c'/c
Leading edge devices	
Fixed slot	0.2
Leading edge flap	0.3
Kruger flap	0.3
Slat	0.4 c'/c

Table 12. Approximate lift contributions of high-lift devices (Raymer Table 12.2).

	Fighters		Transport & Bomber		General aviation		Multiplier	Approximate location
	lb/ft ²	kg/m ²	lb/ft ²	kg/m ²	lb/ft ²	kg/m ²		
Wing	9	44	10	49	2.5	12	$S_{exposed\ planform}$	40% MAC
Horizontal tail	4	20	5.5	27	2	10	$S_{exposed\ planform}$	40% MAC
Vertical tail	5.3	26	5.5	27	2	10	$S_{exposed\ planform}$	40% MAC
Fuselage	4.8	23	5	24	1.4	7	$S_{wetted\ area}$	40–50% length
	Weight ratio	Weight ratio	Weight ratio	Weight ratio	Weight ratio	Weight ratio		
Landing gear*	0.033		0.043		0.057		TOGW	centroid
Landing gear—Navy	0.045		—		—		TOGW	centroid
Installed engine	1.3		1.3		1.4		Engine weight	centroid
"All-else empty"	0.17		0.17		0.1		TOGW	40–50% length

*15% to nose gear, 85% to main gear; reduce gear weight by 0.014 W_0 if fixed gear.

Table 13. Component weight – area ratio table

Weight group	Fudge factor (multiplier)
Wing	0.85 – 0.90
Tails	0.83 – 0.88
Fuselage/nacelle	0.90 – 0.95

Table 8.5: Fudge factors to account for composite materials ([Raymer, 2006](#))

Table 14. Fudge factor for different components.

Aircraft type	Diameter		Width	
	A	B	A	B
British units: Main wheels diameter or width (in.) = AW_W^B				
General aviation	1.51	0.349	0.7150	0.312
Business twin	2.69	0.251	1.170	0.216
Transport/bomber	1.63	0.315	0.1043	0.480
Jet fighter/trainer	1.59	0.302	0.0980	0.467
Metric units: Main wheels diameter or width (cm) = AW_W^B				
General aviation	5.1	0.349	2.3	0.312
Business twin	8.3	0.251	3.5	0.216
Transport/bomber	5.3	0.315	0.39	0.480
Jet fighter/trainer	5.1	0.302	0.36	0.467

Table 15. Tire size table.

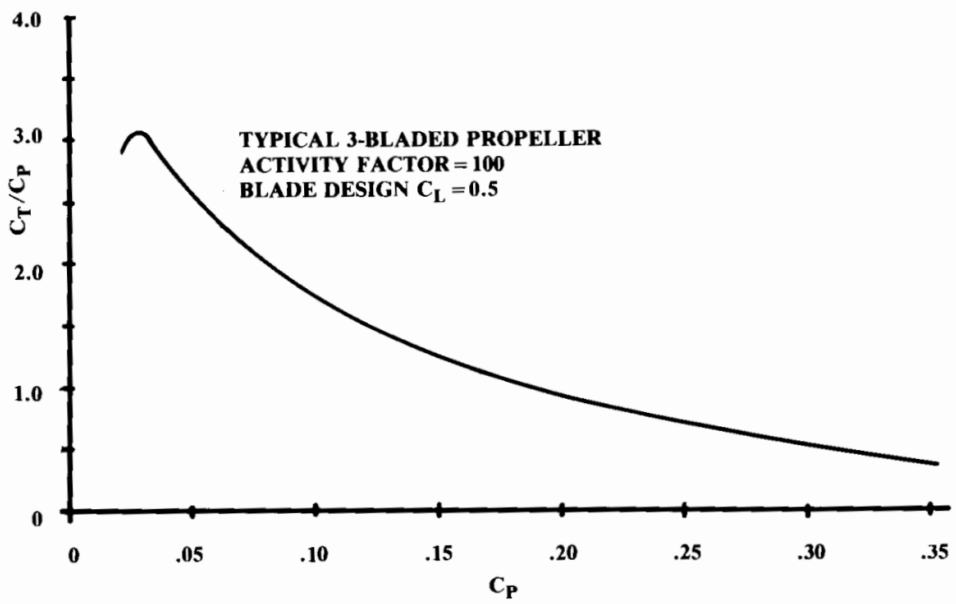


Fig. 13.8 Static propeller thrust. (after Ref. 50)

Figure 59. Power coefficient and thrust coefficient relationship (Raymer).